



**PUMP DIODE CHARACTERIZATION FOR  
AN UNSTABLE DIODE-PUMPED ALKALI  
LASER RESONATOR**

THESIS

Chad T. Taguba, Master Sergeant, USAF  
AFIT-ENP-13-M-33

**DEPARTMENT OF THE AIR FORCE  
AIR UNIVERSITY**

***AIR FORCE INSTITUTE OF TECHNOLOGY***

**Wright-Patterson Air Force Base, Ohio**

**DISTRIBUTION STATEMENT A.  
APPROVED FOR PUBLIC RELEASE; DISTRIBUTION UNLIMITED.**

The views expressed in this thesis are those of the author and do not reflect the official policy or position of the United States Air Force, Department of Defense, or the United States Government. This material is declared a work of the U.S. Government and is not subject to copyright protection in the United States.



AFIT-ENP-13-M-33

PUMP DIODE CHARACTERIZATION FOR AN UNSTABLE DIODE-PUMPED  
ALKALI LASER RESONATOR

THESIS

Presented to the Faculty  
Department of Engineering Physics  
Graduate School of Engineering and Management  
Air Force Institute of Technology  
Air University  
Air Education and Training Command  
in Partial Fulfillment of the Requirements for the  
Degree of Master of Science in Applied Physics

Chad T. Taguba, BS  
Master Sergeant, USAF


March 2013

**DISTRIBUTION STATEMENT A.**  
APPROVED FOR PUBLIC RELEASE; DISTRIBUTION UNLIMITED.

PUMP DIODE CHARACTERIZATION FOR AN UNSTABLE DIODE-PUMPED  
ALKALI LASER RESONATOR

Chad T. Taguba, BS  
Master Sergeant, USAF

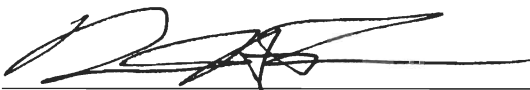
Approved:



Dr Glen P. Perram (Chairman)

7 Mar 13

Date



Col Brian A. Tom (Member)

8 MAR 13

Date



Lt Col Anthony L. Franz (Member)

7 Mar 13

Date

## Abstract

Measurements of wavelength tunability, spectral linewidth, minimum spot size, and  $M^2$  were made for a rubidium diode-pumped alkali laser (DPAL) containing a volume Bragg grating (VBG) for resonator characterization. The output wavelength of the pump diode was measured as a function of volume Bragg grating temperature. A linear relationship was observed that corresponded to an output wavelength range of  $780.08 \text{ nm} \pm 0.01 \text{ nm}$  to  $780.49 \text{ nm} \pm 0.01 \text{ nm}$  with a tuning rate of  $6.1 \text{ pm}/^\circ\text{C}$  for a diode chassis temperature of  $37^\circ\text{C}$ . A fluorescence excitation spectroscopy experiment was used to study the lineshape of the pump diode. Rubidium  $D_1$  fluorescence spectra were recorded as the diode wavelength was scanned across its full range in  $3 \text{ pm}$  steps. The integrated intensities of the  $D_1$  fluorescence peaks were used to generate a wavelength-dependent intensity profile that was fitted to a Lorentzian lineshape with line center at  $780.23 \text{ nm}$  and a FWHM of  $0.12 \text{ nm}$ . A knife-edge experiment measured the power profiles of the pump diode beam along a  $4.5 \text{ cm}$  beam path. The pump diode  $M^2$  was determined by a nonlinear model fit to be 132, resulting in a minimum spot size of  $0.41 \text{ mm}$ . These results enable the pump diode to be matched with a alkali gain media for the validation of unstable DPAL resonator designs.

## Acknowledgements

First, I would like to thank my advisor, Dr. Glen Perram, for his guidance in helping me grok the subtleties and nuances of experimental physics as well as providing perspective when everything seemed lost.

I would also like to thank my fellow students Ben Eshel, 2Lt. Matt Guy, Capt. Chris Vineski, and Capt. Andrew Westman. Amongst the student body, there's a saying: Cooperate to graduate. This journey would have been impossible were it not for their camaraderie.

And last, but not least, I would like to thank Jason and Ted. Without their friendship, wisecracks and unceasing encouragement, I would never have succeeded in this Herculean effort.

Chad T. Taguba

# Table of Contents

	Page
Abstract .....	iv
Acknowledgements .....	v
List of Figures .....	viii
List of Tables .....	ix
I. Introduction .....	1
1.1 Motivation and Background .....	1
1.2 Spectra Physics DPAL Description .....	2
1.3 Research Objective .....	4
1.4 Assumptions and limitations .....	5
1.5 Document Structure .....	6
II. Background .....	7
2.1 Chapter Overview .....	7
2.2 The DPAL Process .....	7
2.3 Gaussian Beams .....	8
2.4 Volume Bragg Gratings and Laser Diodes .....	12
2.5 Laser Resonators .....	15
III. Experiments .....	19
3.1 Chapter Overview .....	19
3.2 VBG Characterization Experiment .....	19
3.3 Pump Beam Waist Characterization Experiment .....	20
3.4 Pump Beam Linewidth Characterization Experiment .....	22
IV. Results and Analysis .....	24
4.1 Chapter Overview .....	24
4.2 VBG Characterization Analysis .....	24
4.3 Pump Beam Waist Characterization Analysis .....	27
Fiber Rotation Dependence .....	29
Translational Corrections .....	29
Beam Waist Determination .....	33
4.4 Pump Beam Linewidth Characterization Experiment .....	34

	Page
V. Conclusions and Recommendations .....	38
5.1 Chapter Overview .....	38
5.2 Conclusions.....	38
5.3 Recommendations for Future Work .....	39
Appendix A. Spectra Physics J80 Diode Controller Operations .....	40
1.1 Communications Settings.....	40
1.2 Commands and Syntax.....	40
Appendix B. Volume Bragg Grating Operations .....	46
2.1 Overview.....	46
2.2 Syntax Issues .....	47
Bibliography .....	50
Vita.....	51

## List of Figures

Figure		Page
1	Spectra Physics DPAL Schematic .....	3
2	Rubidium Gain Cell .....	4
3	Lasing scheme for rubidium .....	8
4	Spectra Physics Pump Diode .....	13
5	Volume Bragg Grating Propagation .....	14
6	Spectra Physics Volume Bragg Grating .....	16
7	Knife Edge Theory .....	21
8	Knife Edge Measurement Apparatus .....	21
9	Linewidth Measurement Apparatus .....	23
10	D1 Fluoresence .....	23
11	Pump Diode Spectral Comparison .....	25
12	Volume Bragg Grating Tunability .....	26
13	Pump Diode Slope Efficiency .....	27
14	Pump Diode Slope Efficiency at 37°C .....	28
15	Effects of Fiber Rotation on Beam Centroid Position .....	30
16	Knife Edge Translational Error .....	31
17	Positional Error Correction in Knife Edge Power Profile Data .....	32
18	Knife Edge Power Profile Comparison for 0° and 90° .....	33
19	Pump Beam Waist Nonlinear Fit .....	34
20	Pump Diode Linewidth Nonlinear Fit .....	37
21	VBG Hyperterminal Command Anomaly Example .....	48

## List of Tables

Table		Page
1	Spectra Physics DPAL Cavity Characteristics .....	18
2	Pump Beam Waist Characterization Results .....	34
3	Pump Beam Linewidth Measurement Results .....	36
4	Spectra Physics DPAL Pump Diode Operating Parameters .....	38
5	Communications Settings for the J80 Controller .....	40



# PUMP DIODE CHARACTERIZATION FOR AN UNSTABLE DIODE-PUMPED ALKALI LASER RESONATOR

## I. Introduction

### 1.1 Motivation and Background

Throughout the years, the DOD has been continuously working towards a practical laser that offers high power, robustness, and minimal logistical support. Technology demonstrators such as the Tactical High Energy Laser, the Airborne Laser Laboratory and the Airborne Laser Test Bed have all pushed the envelope of laser technology and confirmed the feasibility of high-power laser weapon systems. In recent years, lasers using gas-phase alkali gain cells have been used to generate kilowatt-class output (*Bogachev et al.*, 2012). This is sufficient to be considered as the basis for a practical high-energy laser. The diode-pumped alkali laser (DPAL) is a quickly-maturing laser technology that has the potential to become an efficient, high-power, robust laser suitable for military applications.

The DPAL design is a hybrid laser, consisting of a semiconductor laser to excite a gas-phase alkali lasing medium in an optical resonator. Alkali atoms are an attractive candidate for high power outputs since they possess large absorption cross sections and low quantum defects between  $P$  states. The laser diodes are used to excite the alkali atoms from their  $5^2S_{1/2}$  ground state to their second excited state,  $5^2P_{3/2}$ . Collisional relaxation with buffer gases cause the alkali atoms to transition to the  $5^2P_{1/2}$  excited state. Stimulated emission occurs when the alkali atoms de-excite via the  $D_1$  transition to the ground state. By harnessing the high efficiency and power

of modern laser diodes with the high gain of the alkali gain medium, DPAL systems have been demonstrated with slope efficiencies of up to 80% (*Brown and Perram, 2012*).

A limiting factor in the beam quality and amount of power that can be extracted from a DPAL gain cell is its resonator design. Past research has been focused primarily around low power stable resonator configurations as a means to understand the kinetics of the gas-phase alkali media and experiment with pump sources. In these devices, the resonator constrains the pump source to interact with a relatively small volume of the available gain medium, resulting in low mode volumes that do not take full advantage of the potential gain of the alkali medium. Unstable resonators, on the other hand, have an inherent advantage with possessing large mode volumes, enabling the pump source to interact with a larger volume of the gain medium (*Zameroski et al., 2011*). A high-power DPAL could take advantage of the high gain of the alkali gain cell by pairing a high-power pump source with an unstable resonator, thereby maximizing the interacting mode volume of the alkali gain cell.

## 1.2 Spectra Physics DPAL Description

The current resonator design experiments are centered on a prototype DPAL constructed by Spectra Physics in 2009. The layout of the system is shown in Figure 1. A multiple-emitter laser diode with a tunable volume Bragg grating (VBG) is used as a pump source. The diode is coupled to a fiber that terminates on a rotation stage. Laser light emitted from the aperture of the fiber enters a collimation lens, producing a well-collimated beam approximately 2 cm in diameter. The collimated beam passes through a converging lens with a 13 cm focal length and enters a 30 cm semi-hemispherical cavity through a dichroic flat mirror. This flat mirror is coated to allow the pump beam to pass into the cavity while reflecting the rubidium  $D_1$  lasing

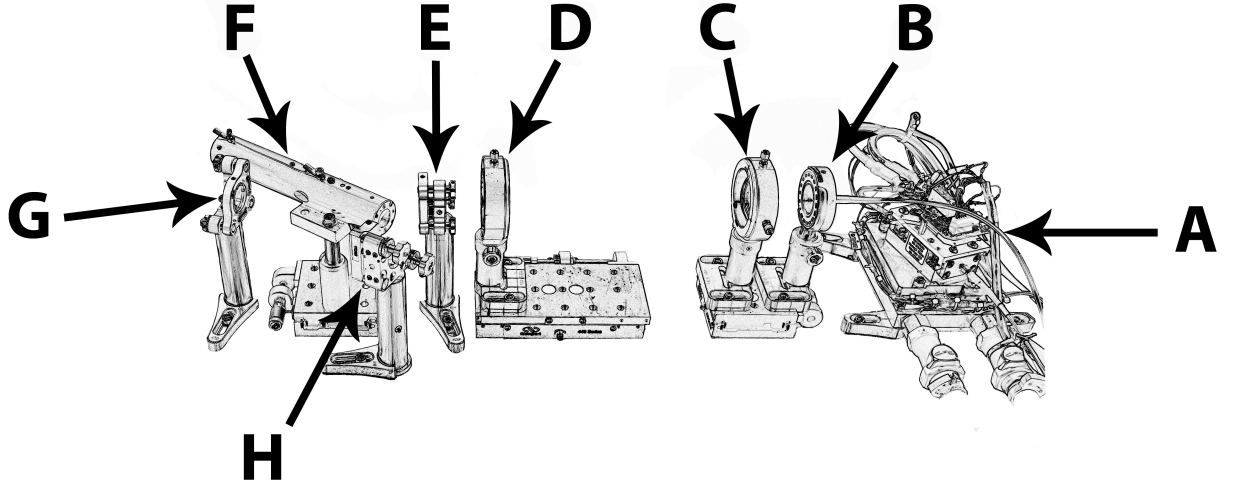


**Figure 1. Spectra Physics DPAL Schematic.** The pump diode *A* generates a continuous wave output at 780 nm at up to 50 W. The diode output is coupled to a fiber that terminates in rotation stage *B*. The beam passes through collimator *C* and focusing lens *D* before entering the cavity through the high reflector *E*. The pump beam is focused to a point in the gain cell, located in the oven *F*, generating a 795 nm beam. The dichroic turning mirror, *G*, reflects the 795 nm beam while allowing the 780 nm pump beam to exit the cavity. The 795 nm beam then exits the cavity through the output coupler *H*.

line. The beam propagates to the gain cell heater block located at the pump waist in the cavity. The heater block is oriented such that the beam encounters the window of the gain cell at the Brewster's angle. After the gain cell, the beams are reflected off a turning mirror that reflects the  $D_1$  lasing line but allows the majority of the pump beam to leave the cavity. The lasing beam then exits the cavity through a dichroic output coupler with 25% transmission and a radius of curvature of 60 cm. The diode is controlled by a Spectra Physics J80 laser diode controller with a special instruction set for DPAL applications. The J80 communicates to the laser diode via serial interface.

The gain cell is a small rubidium gain cell with a narrow interaction length of 5 mm constructed by Spectrocell. Data from Spectra Physics indicated the cell was filled



**Figure 2. Spectra Physics DPAL Gain Cell.** The cell has an overall length of 95 mm, of which 40 mm is the length of the reservoir. It has a height of 12.5 mm, a width of 7.6 mm and a wall thickness of approximately 1.5 mm

with ethane; however, comparing FTIR measurements to the HITRAN database using line-by-line radiative transfer models (LBLRTM) revealed the presence of methane at approximately 1 atm.

### 1.3 Research Objective

The initial approach was to characterize the DPAL in a stable lasing mode as a baseline to compare unstable resonator performance. During an alignment procedure for the stable resonator, one of only two gain cells was destroyed while the diode pump beam was set to 6 W, despite the fact that the gain cells were designed for operation up to 40 W. With only one gain cell remaining, it was decided to fully characterize the pump and resonator before proceeding further. This study seeks to characterize pump diode parameters relevant to the gain cell of the Spectra Physics DPAL. To this end, there are three key characteristics that must be understood. First, the beam waist and its location must be well-known. With pump intensities that have the potential to exceed  $1 \text{ kW/cm}^2$ , the location of the beam waist is critical to prevent

damage to gain cells with millimeter-scale interaction lengths. This data can also be used to determine the operational threshold of the DPAL; particularly, whether or not the pump is capable of generating the intensities required for DPAL operation. Second, the linewidth of the pump diode wavelength must be determined. Knowing the pump linewidth is crucial in both understanding the behavior of the gain cell and in determining the specifications of new gain cells. Last, the wavelength tunability of the volume Bragg grating must be characterized. The absorption linewidth of rubidium is very small, even compared to a Bragg-narrowed linewidth. Learning how to control the tuning range of the VBG will permit the fine-tuning of the output frequency of the pump to match the absorption line of the gain cell.

#### 1.4 Assumptions and limitations

When the Spectra Physics DPAL was delivered in 2009, it was assumed to be aligned and operational. But given the one-of-a-kind nature of the laser, scholarly articles published by Spectra Physics (*Petersen and Lane, 2008*), and the loss of one of only two existing gain cells, the following limitations were set:

1. No physical manipulation of the laser diode can occur.
2. The cavity may not be altered until the diode is characterized.
3. The pump diode has a linewidth of approximately 50 GHz, or 0.1 nm.
4. Beam delivery is made via 400  $\mu\text{m}$  core, 0.22 NA multi-mode optical fiber.
5. The volume Bragg grating has a tunability rate of approximately 7 pm/°C.
6. The volume Bragg grating was constructed by phase hologram recording.
7. The  $M^2$  of the pump is approximately 125.
8. The pump diode is a multiple-emitter design.

## 1.5 Document Structure

This document is organized into five chapters. Chapter II provides background information on the principles of DPAL operation, laser beam characterization, laser diodes with volume Bragg gratings, and laser resonator fundamentals. Chapter III explains the methodology used in each characterization experiment. Chapter IV presents the results of the experiments and a discussion of experimental error. A summary of the results, final conclusions, and recommendations for future work are given lastly in Chapter V.

## II. Background

### 2.1 Chapter Overview

This chapter is devoted to the mathematical explanation of the physical processes that govern how the laser diode output is transformed from a multiple-wavefront, multiple-wavelength beam inside the diode to a finely-tuned, wavelength-narrowed beam converging in the center of a rubidium gain cell. First, an overview of the DPAL pumping scheme will be discussed. Second, a formulation of Gaussian laser beams will establish the language necessary to describe how a laser beam physically behaves as it propagates from the diode to the gain medium and how the beam propagation factor,  $M^2$ , can be used to relate a real non-Gaussian beam into terms of a more manageable Gaussian description. Next, the properties the Spectra Physics DPAL pump diode will be discussed. In particular, the fundamentals of the internal volume Bragg grating will be explored to understand how a beam consisting of the output of multiple diode emitters can be shaped to fit the needs of a DPAL. Next, the key parameters of a semi-hemispherical optical resonator will be explored with an emphasis on mode volumes.

### 2.2 The DPAL Process

Alkali atoms possess a single electron in their valence shell. In the case of rubidium, the electron configuration of the ground state is  $5^2S_{1/2}$ . The excited  $P$  state consists of two states,  $5^2P_{1/2}$  and  $5^2P_{3/2}$  due to spin-orbit splitting. In  $^{87}\text{Rb}$ , the quantum efficiency between the  $P_{3/2,1/2}$  states is high at 0.981 (*Krupke et al.*, 2003) with a spin-orbit splitting energy difference of  $237\text{ cm}^{-1}$  (natural rubidium will also exhibit hyperfine splitting due to the presence of  $^{85}\text{Rb}$ ). Coupled with an absorption cross section on the order of  $10^{-13}\text{ cm}^2$ , a rubidium gain cell can produce more than  $10^8$

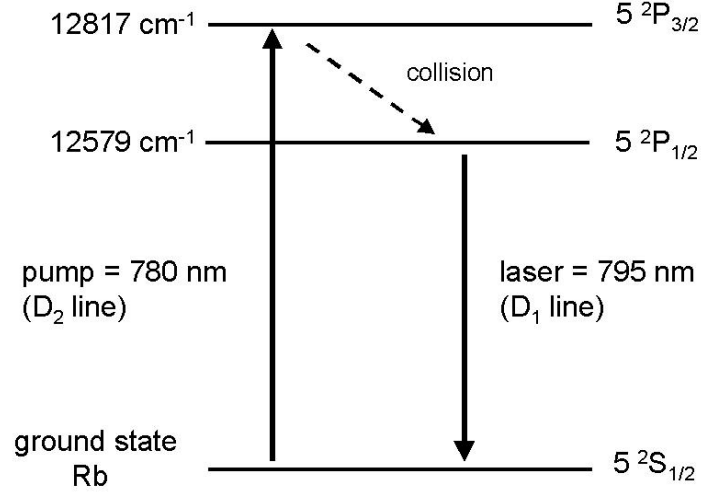


**Figure 3. Lasing scheme for rubidium.** Atoms excited by the pump beam transition to  $5^2P_{3/2}$  and undergo collisional interactions with the buffer gas and relax to the  $5^2P_{1/2}$  state. The atoms then lase via the  $D_1$  line back to the ground state.

photons per second for every excited atom. This gives a rubidium gain cell a very high energy density; therefore, large volumes are not needed to produce high powers.

To produce the excited atoms, the rubidium is placed in a sealed gain cell and heated to produce rubidium vapor. This vapor is optically pumped by a laser diode tuned to emit at the energy of the  $D_2$  transition, thereby exciting the rubidium to the  $5^2P_{3/2}$  state. Helium is added to collisionally broaden the the absorption cross section of the rubidium atoms and promote excitation. This is crucial since the natural absorption linewidth can be several orders of magnitude smaller than the spectral width of the pump source. The DPAL lasing scheme is shown in Figure 3.

### 2.3 Gaussian Beams

For the laser beams and optical cavities used in this thesis, it is necessary to have a method to describe the laser beams that provides crucial information about their state and behavior. Laser beams are commonly described using Gaussian waves for



their ability to generate good approximations of beam intensity distributions and their ease of computation (the transform of a Gaussian is another Gaussian). By expressing the laser beams in terms of a Gaussian wave, two key beam parameters, the beam waist and characteristic length parameter (or Rayleigh range), are obtained that can be used to derive any characteristic of the Gaussian beam. For a beam propagating along the  $z$ -axis, its electric field can be expressed as

$$\mathbf{E}(\mathbf{r}, t) = E_0 \psi e^{i((k_x \hat{x} + k_y \hat{y} + k_z \hat{z}) \cdot \mathbf{r} - \omega t + \phi)} \approx E_0 \psi e^{i(kz - \omega t + \phi)} \quad (1)$$

where  $E_0$  is the amplitude of the electric field,  $\psi$  is the spatial intensity distribution of the field,  $\omega$  is the frequency of the wave,  $t$  is time,  $\phi$  is the global phase factor,  $\mathbf{k}$  is the propagation vector, and  $|k_x \hat{x} + k_y \hat{y}| \ll |k_z \hat{z}|$ . The behavior of the wave as it circulates in a simple cavity can be described using the paraxial Helmholtz equation:

$$\nabla_T^2 E_0 \psi_0 + i2k \frac{\partial}{\partial z} E_0 \psi_0 = 0 \quad (2)$$

where  $\nabla_T^2$  is known as the *transverse Laplacian*. The paraxial Helmholtz equation is an important result because it relates the transverse intensity distribution of the beam to the diffraction losses as the beam propagates through space.

Up to this point,  $\mathbf{E}(\mathbf{r}, t)$  is still nothing more than a slightly modified plane wave with assumptions. The equation of the wave must be able to describe the cross sectional amplitude while taking into account the effects of the diffraction at the beam's boundary. By using a Gaussian intensity distribution for  $\psi_0$ , the laser beam can be expressed as a Gaussian wave.

$$\psi_0 = e^{-\left(\frac{kz_0 r^2}{2(x^2 + z_0^2)}\right)} e^{-i\left(\frac{kz r^2}{2(x^2 + z_0^2)}\right)} e^{-iP(z)} \quad (3)$$

Using the paraxial Helmholtz equation, the solution to the electric field is shown in

Equation 4 (Verdeyen, 1995):

$$\frac{E(x, y, z)}{E_0} = \frac{w_0}{w(z)} e^{-\left(\frac{r^2}{w^2(z)}\right)} e^{-i\left(kz - \arctan\left[\frac{z}{z_R}\right]\right)} e^{-i\left(\frac{kr^2}{2R(z)}\right)} \quad (4)$$

where  $w_0$  is the minimum spot size (or beam waist) of the beam,  $r$  is the distance from the center of the beam,  $w(z)$  is the radius of the beam at some distance  $z$ ,  $R(z)$  is the complex radius of curvature of the wavefront of the beam, and  $z_R$  is the characteristic length parameter. Equation 4 describes a Gaussian beam with only one mode of oscillation in the amplitude cross section, also known as a TEM<sub>00</sub> laser beam and the parameters are listed below. This beam is considered a baseline from which other beams may be compared. Verdeyen uses the following definitions for Equation 4

$$R(z) = z \left[ 1 + \left( \frac{\pi n w_0^2}{\lambda_0 z} \right)^2 \right] = z \left[ 1 + \left( \frac{z_R}{z} \right)^2 \right] \quad (5)$$

$$w^2(z) = w_0^2 \left[ 1 + \left( \frac{\lambda_0 z}{\pi n w_0^2} \right)^2 \right] = w_0^2 \left[ 1 + \left( \frac{z}{z_R} \right)^2 \right] \quad (6)$$

$$z_R = \frac{\pi n w_0^2}{\lambda_0} \quad (7)$$

The quantity  $z_R$  is known as the *Rayleigh range* and is a measure of the distance along the  $z$ -axis from the minimum spot size,  $w_0$ , to where the radius  $w(z)$  increases by a factor of  $\sqrt{2}$ . This Gaussian approximation can be successfully used to describe real laser beams that behave like TEM<sub>00</sub> Gaussian beams when in fact they are not. For instance, the output of a multiple-emitter laser diode can be shaped to behave like a Gaussian beam even though it possesses multiple transverse modes of oscillation (Siegman, 1993). The degree to which a real beam differs from the ideal TEM<sub>00</sub> beam is quantified by the *beam propagation factor*,  $M^2$  (often referred to simply as “M-squared”). If  $w_{0(\text{actual})}$  is the actual minimum spot size of a laser beam obtained

by experiment, it can be considered to be a magnification of the theoretical minimum spot size,  $w_{0(\text{Gaussian})}$ , so  $w_{0(\text{real})} = Mw_{0(\text{Gaussian})}$  and the actual Rayleigh range of the laser becomes

$$z_{R(\text{real})} = \frac{\pi n w_{0(\text{real})}^2}{\lambda_0} = \frac{\pi n w_{0(\text{Gaussian})}^2}{\lambda_0 M^2} \quad (8)$$

Similarly, the waist  $w(z)$  becomes

$$w_{(\text{real})}^2(z) = \left[ M^2 + M^2 \left( \frac{\lambda_0 z}{\pi n w_0^2} \right)^2 \right] w_{0(\text{Gaussian})}^2 = \left[ M^2 + M^2 \left( \frac{z}{z_R} \right)^2 \right] w_{0(\text{Gaussian})}^2 \quad (9)$$

Thus, a Gaussian or Gaussian-like beam can be characterized by two experimentally-derived parameters: the size and location of the beam waist. There are a number of methods to obtain these two experimental parameters, such as the knife-edge test. The definition of the beam waist,  $w_0$ , is somewhat arbitrary but for the purposes of this experiment, the waist was determined according to ISO 11146, which defines the beam waist as the location along the  $z$ -axis where the beam intensity falls to  $1/e^2$ . For a Gaussian-like beam, Verdeyen approximates the intensity profile as

$$I \approx |E_0(r)| e^{-\left(\frac{2(x^2+y^2)}{w^2}\right)} = I_0 e^{-\left(\frac{2x^2}{w^2}\right)} \quad (10)$$

By integrating this along the  $x$ - and  $y$ -axes, power distribution across the beam profile can be found. Along the  $x$ -axis, the beam power is given by

$$P_x = P_{\text{total}} - I_0 \sqrt{\frac{\pi w^2}{2}} \int_{-\infty}^{x'} e^{-\left(\frac{2x^2}{w^2}\right)} dx \quad (11)$$

where  $I_0$  is the initial intensity,  $w$  is the spot size,  $x'$  is the beam center, and  $P_{\text{total}} = \frac{\pi w^2}{2} I_0$ . Using the Gaussian error function identity  $\text{Erf}(t) = \frac{2}{\sqrt{\pi}} \int_0^t e^{-(t')^2} dt'$ , the  $x$ -axis

power is

$$P_x = \frac{\pi w^2}{4} I_0 \left( 1 + \text{Erf} \left( \frac{x' \sqrt{2}}{w} \right) \right) \quad (12)$$

The above equation can be used to obtain a nonlinear fit to experimentally-obtained power data. A best fit is obtained when the power is normalized and the beam center,  $x'$ , is allowed to vary:

$$\frac{P_x}{P_{total}} = P_{x(normalized)} = \frac{\beta}{2} \left( 1 + \text{Erf} \left( \frac{(x - x') \sqrt{2}}{w} \right) \right) \quad (13)$$

A value for the waist is obtained by using the normalized total power,  $\beta$ , the beam center,  $x'$ , and the waist,  $w$ , as fit parameters. The parameter  $\beta$  is not essential; however, it does serve as a validity test on the fit. If  $\beta \approx 1$ , the fit confidence is high. The  $w(z)$ 's obtained by this method can be used to determine the minimum spot size,  $w_0$ , and its location,  $z_0$ , by performing a nonlinear fit to a plot of  $w(z)$  vs  $z$ .

## 2.4 Volume Bragg Gratings and Laser Diodes

The Spectra Physics DPAL pump diode shown in Figure 4 is designed to produce a non-Gaussian Gaussian (*Siegman*, 1986), where the intensity profile resembles a Gaussian intensity profile but contains more than the TEM<sub>00</sub> mode. The  $\sim 780$  nm laser light is generated by an array of semiconductor junction emitters. Due to the scale and construction of the cavities, the raw beam is highly elliptical and diverges quickly along the  $x$ -axis, also known as the fast axis. The beam then passes immediately into an optical element known as a beam twister. A beam twister consists of an array of microlenses that correct the fast-axis divergence of each emitter and rotates each emitter beam around the optical axis to improve the collimation of the beam. A series of focusing lenses launches the collimated beam into the optical fiber.

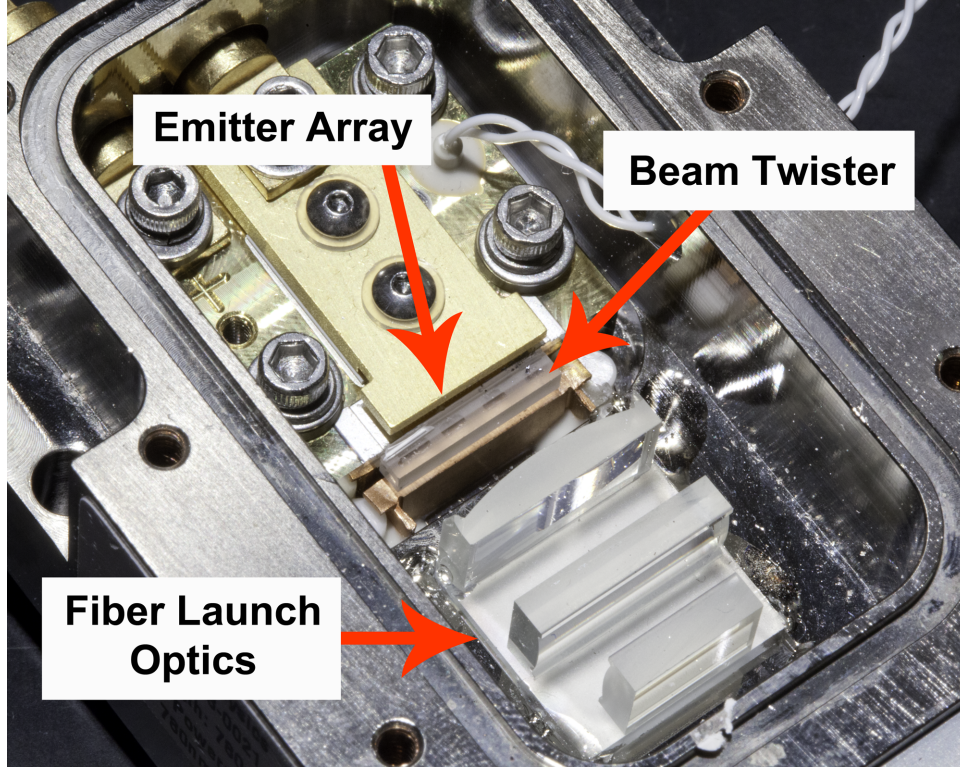


Figure 4. Internal configuration of the Spectra Physics pump diode.

The spectral linewidth of a laser diode can be on the order of several nanometers. When using the laser diode output as a pumping source for a gain medium such as a gas-phase alkali cell, much of the pump power is wasted because the absorption linewidth of the alkali cell is several orders of magnitude smaller. For instance, the FWHM of the absorption line of a simple, pressure-broadened rubidium cell with a 500 Torr krypton buffer gas at 394 K is  $\sim 0.017$  nm. Without narrowing the linewidth of the pump source, much of the pump power is wasted. A volume Bragg grating can significantly narrow the linewidth of the pump diode beam. Constructed from photothermoreactive (PTR) glass, the VBG possesses a periodically-varied index of refraction with a  $|\cos \theta_m^*| = \lambda f / 2n_{av}$  Bragg condition, where  $n_{av}$  is the average index of refraction for the grating,  $\lambda$  is the incident wavelength,  $f = 1/\Lambda$  is the spatial frequency of the index variation, and  $\theta_m^*$  is the angle formed between diffracted beam and a plane of constant  $n$  as shown in Figure 5. The angle  $\theta_m^*$  is also known as the

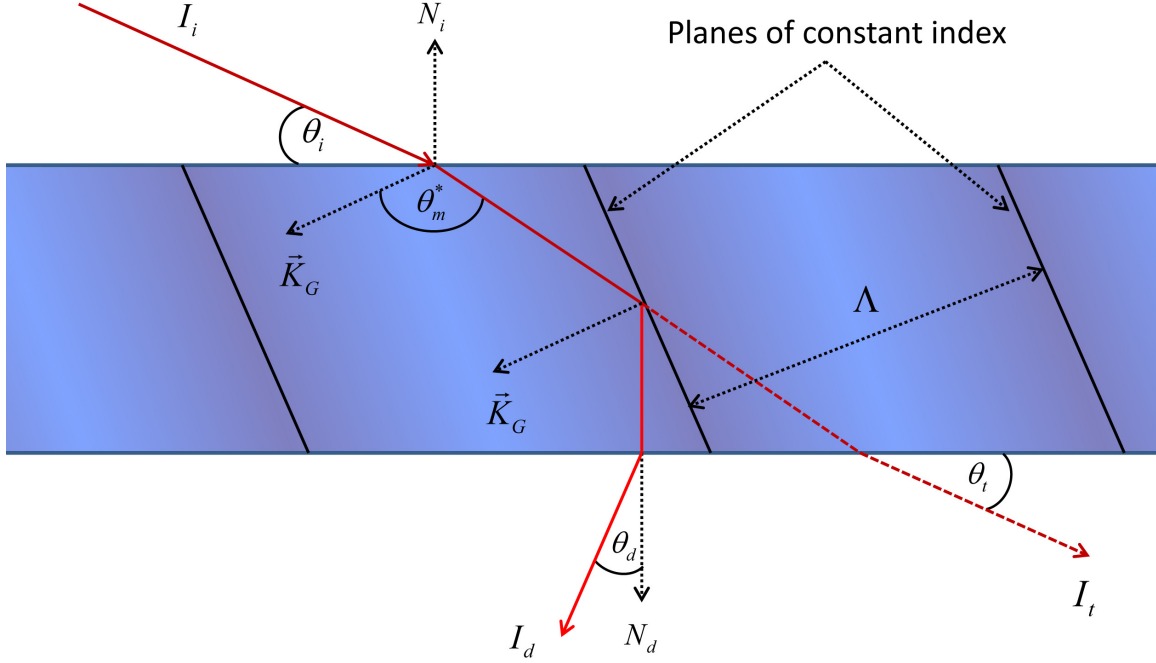


Figure 5. Propagation of a beam through a volume Bragg grating. For a transmission VBG, an incident monochromatic wave  $I_i$  with a finite linewidth enters the VBG at an angle  $\theta_i$  and encounters planes of constant refractive index spaced  $\Lambda$  apart. Wavelengths that satisfy the Bragg condition are diffracted out of the VBG at an angle  $\theta_d$  and intensity  $I_d$ . Wavelengths that do not satisfy the Bragg condition continue through the crystal and exit with an intensity  $I_t$  at an angle equal to the incidence angle.  $N_i$  and  $N_d$  are surface normals and  $K_G$  is the grating vector normal to the plane of constant index. Adapted from Ciapurin, et al., 2005.

incident Bragg angle.

The performance of the grating is characterized by its angular and spectral selectivities. The selectivities set upper and lower bounds on what incidence angles and wavelengths satisfy the Bragg condition. Modeling by Ciapurin, et. al, showed the diffraction efficiency,  $\eta_\theta(b)$ , of a VBG for a Gaussian input beam with normal incidence can be given by Equation 14 (Ciapurin et al., 2005):

$$\eta_\theta(b) = \sqrt{\frac{2}{\pi b}} \int \eta(\theta) e^{-2\left(\frac{\theta - \theta_m}{b}\right)^2} d\theta \quad (14)$$

where  $\eta(\theta)$  is the angular-selectivity-dependent diffraction efficiency of the VBG,  $\theta$  is the angle of diffraction and  $\theta_m$  is the conventional Bragg angle. The conventional

Bragg angle is related to the incident Bragg angle by  $|\cos \theta_m^*| = \sin \theta_m$ . The parameter  $b$  is the beam divergence and is given by  $b = \frac{2\lambda_0}{\pi D}$ , where  $\lambda_0$  is the vacuum wavelength of the input beam and  $D$  is the diameter of the input beam. When a beam enters the VBG, only those wavelengths that satisfy the Bragg condition are diffracted. Wavelengths that do not satisfy the Bragg condition continue unimpeded and exit the crystal at the angle of incidence. For a Gaussian beam, these "discarded" wavelengths are in the wings of the lineshape distribution. This effectively narrows the spectral linewidth of the beam.

In addition to narrowing the linewidth of the input beam, the VBG can also be used to tune the Bragg wavelength. PTR glass exhibits a temperature-dependent wavelength sensitivity of  $7 \text{ pm}/^\circ\text{C}$  (*Glebov et al.*, 2012). This allows the VBG to fine-tune the wavelength of the output beam. For a DPAL, this is crucial to achieve the greatest overlap between the absorption and pump diode lineshapes.

In practice, the VBG is mounted on a rotation stage as seen in Figure 6 and placed between the beam twister and fiber launch optics in the diode chassis. To set the output wavelength of the diode, the VBG is first tuned by adjusting the angle of incidence to match the output wavelength to the  $D_2$  transition of rubidium. Fine tuning is accomplished by adjusting the temperature of the VBG. For the Spectra Physics pump diode, the VBG was designed to produce an output linewidth of  $0.1 \text{ nm}$ . This cannot be directly verified since the raw output from the diode emitters cannot be measured.

## 2.5 Laser Resonators

A rubidium DPAL is a three-level laser system, where the population inversion is measured with respect to the ground state. In order to maintain the inversion, high pump intensities are required, with a lower bound of approximately  $300 \text{ W}/\text{cm}^2$

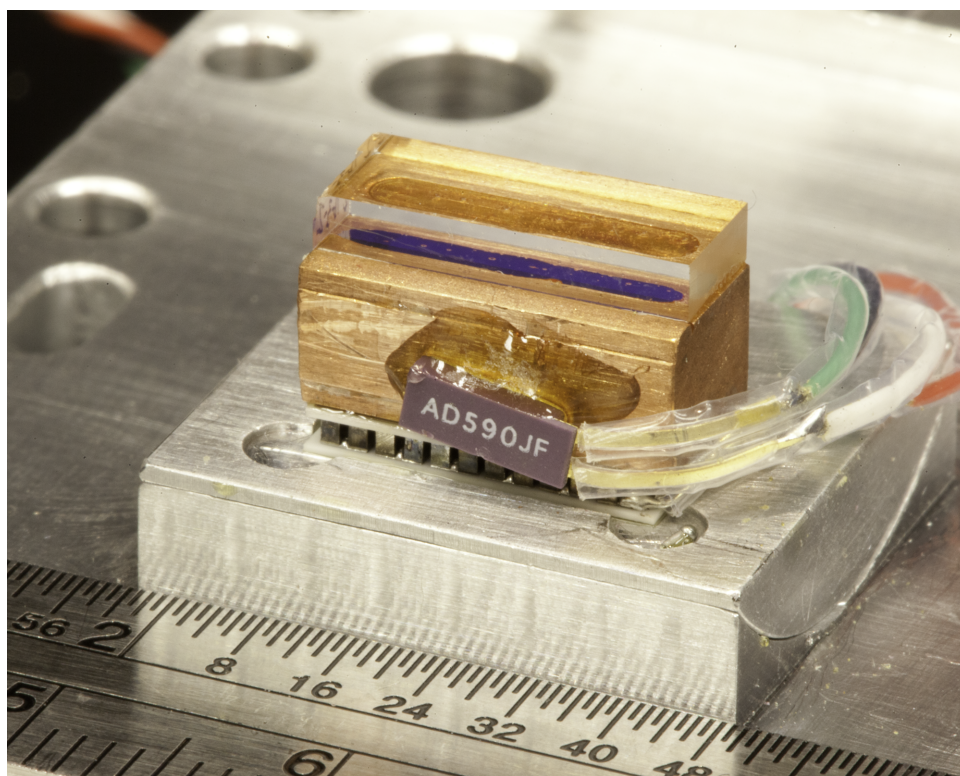


Figure 6. Spectra Physics volume Bragg grating. The grating is mounted on a thermoelectrically-controlled copper block. The component labeled AD590JF is a temperature sensor.



(Hager and Perram, 2010). The cavity design can be configured to match the pump diode to the gain medium and achieve the necessary pumping intensity. The Spectra Physics DPAL is built around a semi-hemispherical cavity with a length of 30 cm and an output coupling mirror with a radius of curvature of 60 cm. The layout is shown in Figure 1, consisting of items E, F, G and H.

In a semi-hemispherical resonator, photons circulate between a mirror with infinite curvature and one with finite curvature. By matching the phase of a Gaussian wave inside the cavity to the phase surfaces of the mirrors, the size and location of the beam waist can be found. By setting the high reflector at the arbitrary  $z$ -axis position of  $z = 0$ , the curvature of the Gaussian wave is equal to the curvature of the mirror, or flat. Similarly, the Gaussian wave can be matched to the output coupler, which has a radius of curvature of  $R_{OC} = 30$  cm, and obtain the Rayleigh range,  $z_R$ , by using Equation 5:

$$R_{OC} = d \left[ 1 + \left( \frac{z_0}{z} \right)^2 \right] \rightarrow z_0 = \sqrt{dR_{OC} - z^2} \quad (15)$$

where  $z$  is equal to the cavity length. In turn, this can be used to obtain the size of the beam waist,  $w_0$  using Equation 15:

$$z_0 = \frac{\pi n w_0^2}{\lambda_0} \rightarrow w_0 = \sqrt{\frac{\lambda_0 z_0}{\pi n}} \quad (16)$$

The size of the spot at the two mirrors can now be determined with Equation 16. Knowing this, it is now possible to determine the mode volume of the cavity. The mode volume of the cavity is important because it is a measure of how many atoms are lasing in a particular transverse electromagnetic mode. Verdeyen gives the mode volume of a stable cavity as:

$$V_{m,p} = \int_0^d \frac{\pi w_0^2}{2} dz \left( \int_{-\infty}^{\infty} H_m^2(u) e^{-u^2} 2du \right) \left( \int_{-\infty}^{\infty} H_p^2(u) e^{-u^2} 2du \right) \quad (17)$$

where  $d$  is the length of the cavity,  $u$  is a substitution given by  $u = x \sqrt{2}/w$ , and  $m$  and  $p$  relate to the order of the Hermite polynomial  $H$ . This simplifies to

$$V_{m,p} = \frac{\pi w_0^2}{2} d(m!p!2^{m+p}) \quad (18)$$

Using these relationships, the Spectra Physics DPAL cavity has the parameters shown in Table 1. The small scale of the mode volume is from the wavelength dependence of the beam waist and the geometry of the stable cavity. In a stable cavity, photons entering the cavity normal to the plane of the mirrors are restricted to oscillating close to the optical axis, limiting the beam waist. This results in comparatively low output powers, especially from a high-energy laser application perspective. On the other hand, an unstable resonator allows photons in the cavity to “walk off” the optical axis. This allows unstable resonators to have much larger beam waists, greater mode volumes and, consequently, higher output powers.

**Table 1. Spectra Physics DPAL Cavity Characteristics**

Characteristic	Experimental Value
Mode Volume, TEM <sub>00</sub>	0.036 cm <sup>3</sup>
Spot Size at High Reflector (HR)	0.28 mm
Spot Size at Output Coupler (OC)	0.39 mm
Waist, $w_0$ (mm)	0.28 mm
Waist Location (z=0 cm at High Reflector)	0 cm
Rayleigh Range	30 cm

## III. Experiments

### 3.1 Chapter Overview

This chapter describes the methods and experiments used to characterize the Spectra Physics DPAL pump diode. The laser was supplied with no operations manual and extremely sparse technical data. The first few experiments were centered on determining how to operate the laser. The findings of these experiments influenced the subsequent series of experiments. The first section details the volume Bragg grating characterization experiment. The second section describes the beam waist experiment and the last section describes the linewidth experiment.

### 3.2 VBG Characterization Experiment

Early phases of this experiment for this laser centered around obtaining basic characteristics of the pump diode and reverse engineering the command protocol for the VBG. During this time, measurements of the slope efficiency and spectral content of the diode output were taken. Once the VBG command protocol was determined, its tuning range was determined by recording the wavelength of the pump output while the VBG was scanned in  $0.5^{\circ}\text{C}$  increments across a range of  $15^{\circ}\text{C}$  and  $80^{\circ}\text{C}$ , corresponding to steps of  $0.003\text{ nm}$  across a range of  $780.08\text{ nm}$  to  $780.473\text{ nm}$ . The lower bound of  $15^{\circ}\text{C}$  was chosen to minimize the possibility of condensation forming on the VBG surface. The step resolution was chosen based on the resolution of the Bristol 621A wavemeter. The Bristol 621A wavemeter was selected due to the fact that it was the only instrument available that possessed sufficient bandwidth to observe a laser with an anticipated linewidth near  $50\text{ GHz}$ , operating with a degraded resolution of  $0.01\text{ nm}$ . A 70%-30% beamsplitter was placed after the turning mirror. The 70% beam continued along the pump beam propagation axis to a Bristol 621A

wavemeter and the 30% beam was sent to a Coherent FieldMax laser power meter with a PowerMax pyrometer rated for 50 W. Diode chassis and VBG temperatures were recorded by polling the temperature controller on the J80 diode controller. All instrument data was recorded simultaneously using manufacturer-supplied software running under a script manager that automated data collection. The VBG temperature was controlled by sending digital-to-analog controller commands to the J80 diode controller.

### 3.3 Pump Beam Waist Characterization Experiment

The most expeditious method to obtain beam waist data would have been to use a beam profiler such as a Modemaster. This would have required the Modemaster to be placed in the DPAL cavity. Unfortunately, the physical layout of the cavity was too small to accommodate the Modemaster apparatus. The beam could not be redirected out of the cavity for analysis primarily because it would require the use of additional lenses and mirrors and, as such, would no longer be directly measuring the waist in the cavity; rather, it would be measuring the waist of the transform of the optical element nearest the Modemaster. However, the key reason a Modemaster-type instrument was not practical is that even at threshold, the pump diode was sufficiently powerful to damage the detector element.

Instead, a knife-edge experiment was conducted to obtain the necessary data. Figure 7 shows a schematic of a simple knife-edge experiment. After removing the heater block from the cavity, a razor blade was mounted on an  $x$ - $z$  translation stage and placed in the optical path near the  $z$ -location of the cell. The plane of the blade was oriented normal to the optical axis and stepped across the  $x$ -axis cross section of the pump beam in 0.5 mm increments. At each step, the transmitted beam power was measured by a Coherent FieldMax laser power meter with a PowerMax pyrometer

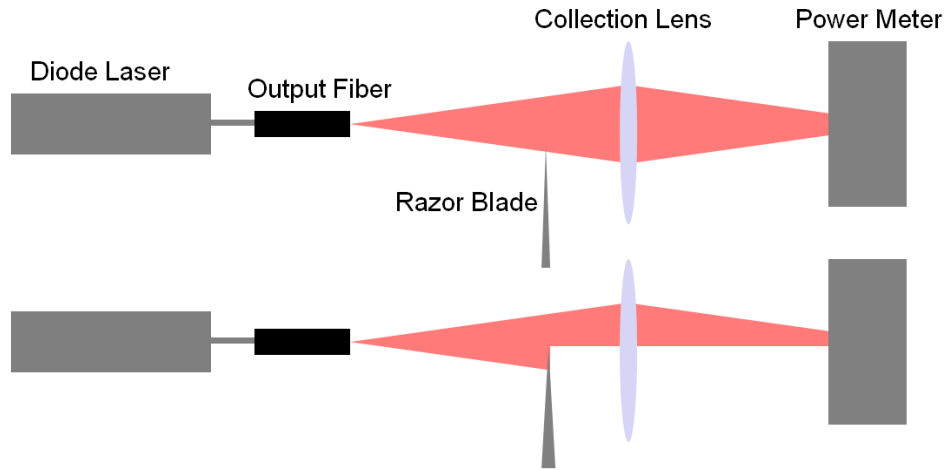


Figure 7. Knife edge theory. The razor blade is incrementally advanced into the beam path. The measured transmitted power is used to build an intensity profile of the beam.

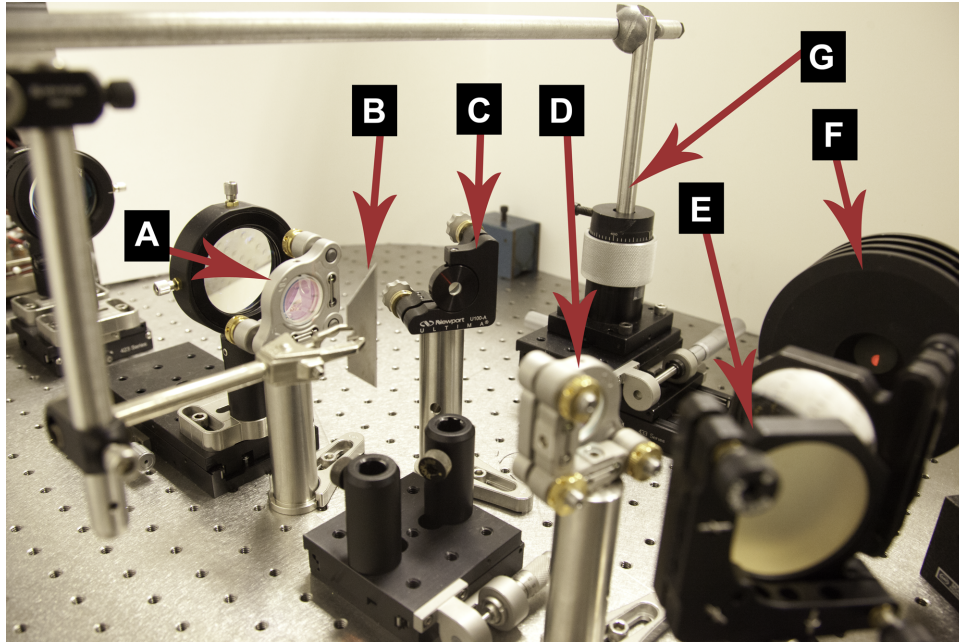


Figure 8. Knife edge apparatus. The pump beam entered the cavity via the high reflector, *A*, intersecting with the blade, *B*. The attenuated beam then passes through the turning mirror, *D*, and is reflected into the power meter head, *F*, by mirror *E*. The output coupler, *C*, is labeled for clarity. Note the partially blocked beam on the face of the power meter head.

rated for 50 W. Transmission power profiles were obtained every 5.0 mm along a 45.0 mm length of the cavity for a total of 10 profiles. The  $z$  translation length of 45 mm was dictated by the mechanical limits of the translation apparatus. The experimental layout is detailed in Figure 8.

### 3.4 Pump Beam Linewidth Characterization Experiment

The linewidth of the pump diode was obtained through a side-fluorescence experiment. To prevent inadvertently damaging the remaining Spectra Physics test cell, a rubidium test cell was used. The test cell contained krypton gas at 500 Torr to act as a collisional partner to obtain  $D_1$  fluorescence. Figure 9 shows how the original Spectra Physics heater block was replaced with a heater block designed for the test cell. The heater block was positioned so the pump beam waist was contained within the test cell, allowing direct observation of the beam waist, which can be seen in Figure 10.

The pump diode chassis was set to an operating temperature of 37°C. Using a fiber-coupled collimator, an Ocean Optics spectrometer with 0.25 nm resolution was used to measure the side fluorescence spectrum. The power transmitted through the test cell was monitored by a laser power meter. The VBG then scanned the pump diode across its entire band, from 780.08 nm to 780.473 nm, in 0.003 nm steps. This was repeated for test cell temperatures of 100°C, 105°C, 110°C and 115°C. The VBG lower bound of 780.08 nm (corresponding to a VBG temperature of 15°C) was chosen to avoid possible condensation issues in the diode. Wavelength data was not directly measured due to the mechanical failure of the Bristol 621A wavemeter. Diode chassis and VBG temperatures were recorded by polling the temperature controller on the J80 diode controller. Instrument data was recorded simultaneously using manufacturer-supplied software running under a script manager that automated data collection.

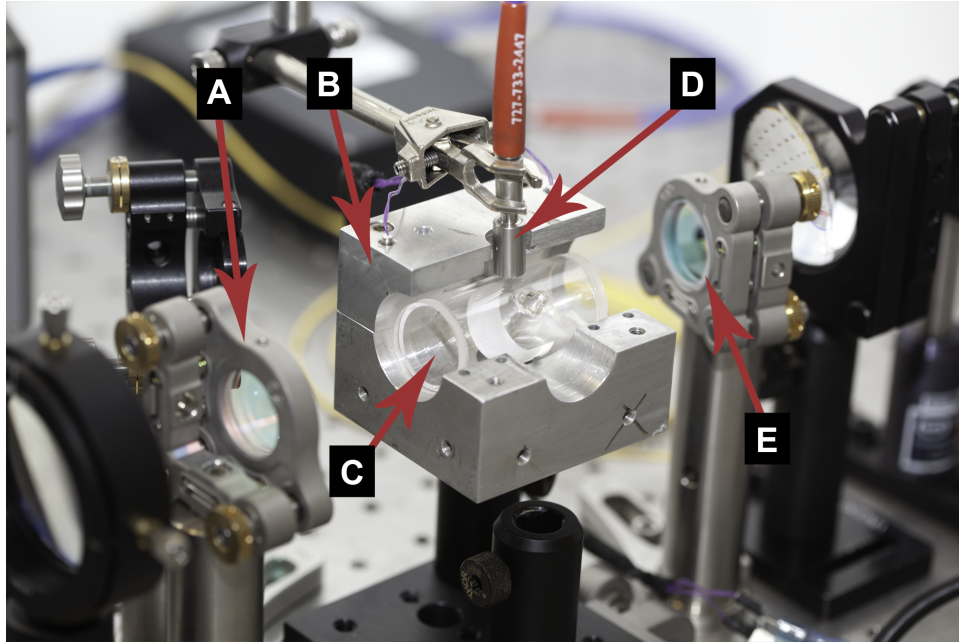


Figure 9. Linewidth apparatus. The laser entered the cavity via the high reflector, *A*, and enters the Rb test cell, *C*, located in heater block *B*. Fluorescence was measured using a fiber-coupled Ocean Optics spectrometer, *D*. The beam exits the cavity at the turning mirror, *E*, and is measured by a laser power meter (not shown).

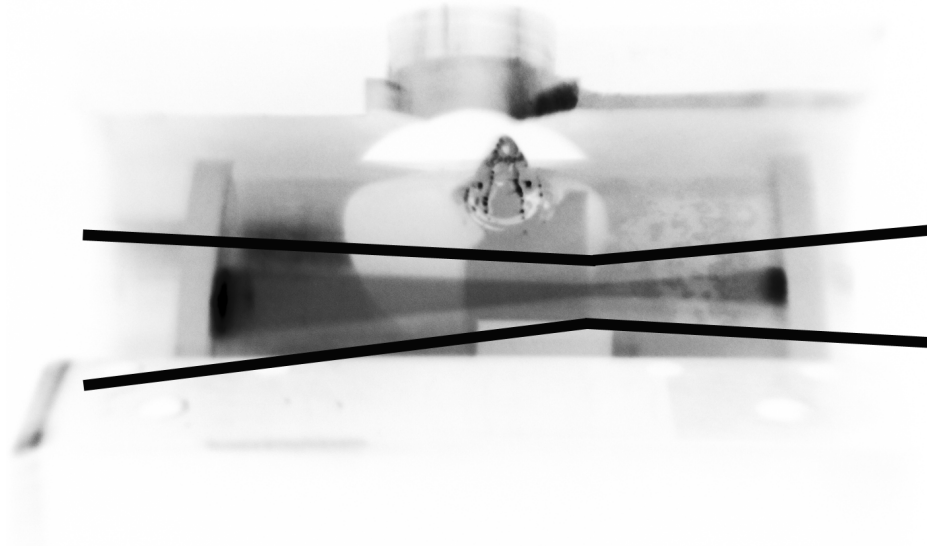


Figure 10. Fluorescence of the D1 line in rubidium. The waist of the pump beam can be clearly seen in the rubidium test cell.

## IV. Results and Analysis

### 4.1 Chapter Overview

The objective of this research was to characterize the pump diode of a DPAL as part of a larger effort to increase DPAL output powers using unstable resonators. The results and analyses in this section will be used to configure the Spectra Physics DPAL for unstable resonator operation. This section is divided into three sections that correspond to the three experiments conducted on the pump diode. The first section presents the results from the volume Bragg grating characterization experiment. The second section details the results from the beam waist experiment and the third section covers the results from the pump diode linewidth experiment.

### 4.2 VBG Characterization Analysis

Initially, the diode chassis temperature was set to 20°C and VBG wavelength data was collected with the Bristol wavemeter. The wavemeter would frequently lose its lock on the output wavelength, especially towards the lower VBG temperatures. An examination of the spectrum of the VBG output with an Ocean Optics spectrometer revealed two peaks of near equal amplitude at  $\sim 780$  nm and  $\sim 772$  nm, shown in Figure 11. The peak wavelength estimates are based on highest intensity. The multiple peaks caused the Bristol wavemeter to dither between the two peaks, resulting in incorrect readings or data dropouts. By raising the diode chassis temperature, the peak centered at  $\sim 780$  nm remained stationary while the peak centered near 772 nm rose in wavelength linearly with temperature.

As the diode chassis temperature changes, the lengths of the individual emitter cavities in the diode change and minute variations in the diode emitter array construction become apparent as they begin to emit at different wavelengths. At the



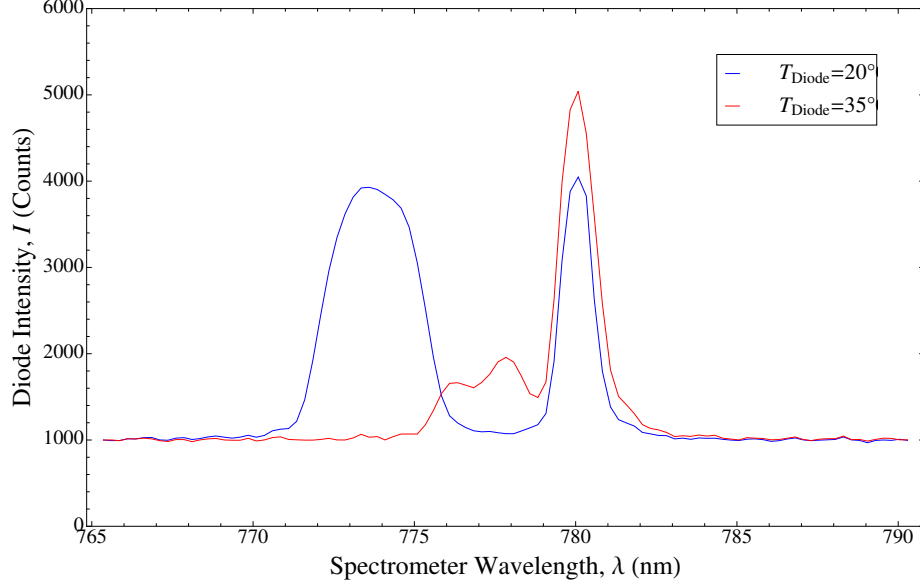


**Figure 11. Comparison of pump diode spectra at different chassis temperatures. As the temperature of the diode chassis is changed from 20 °C to 35 °C, individual emitters in the diode change in length causing the peak centered at  $\sim 772$  nm to merge in to the peak centered at 780 nm.**

upper end of the diode chassis temperature scale, the peaks merge together into a fairly well-defined, single peak. This was best observed at  $\sim 37^\circ\text{C}$ . Finer temperature tuning of the diode chassis temperature was not possible. From this, the diode was set to  $37^\circ\text{C}$  for the remainder of the experiments. It should be noted the higher temperature spectrum in Figure 11 is for  $35^\circ\text{C}$  and not  $37^\circ\text{C}$ . At the time of this particular measurement, the J80 temperature controller was behaving erratically and could not be taken higher than  $35^\circ\text{C}$  before undergoing a runaway temperature rise to the safety thermal cutoff temperature of  $44^\circ\text{C}$ . However, the experimental data used for the fits were for diode chassis temperatures of  $20^\circ\text{C}$  and  $37^\circ\text{C}$ . Once the diode chassis temperatures were set, the Bristol 621A wavemeter was used to record wavelength data as the grating was scanned over its temperature range. A linear fit to the  $37^\circ\text{C}$  experimental VBG data yields

$$\lambda_{\text{exp}(37^\circ\text{C})} = 779.99\text{nm} + (6.05 \times 10^{-3}\text{nm}/^\circ\text{C})T \quad (19)$$

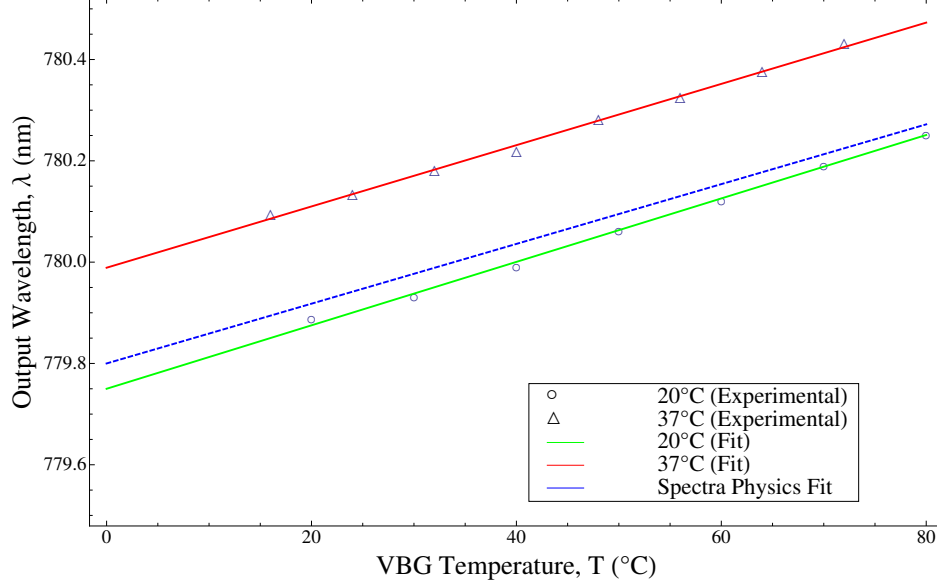


**Figure 12. Volume Bragg grating tuning range.** As the VBG temperature increases from 0°C to 80°C, the output wavelength increases at a rate of 6.7 pm per °C for an operational diode chassis temperature of 37°C. The temperature of the diode chassis for the Spectra Physics fit is not known.

The experimental data is in close agreement with the sparse test data provided by Spectra Physics. The experimental slopes compare favorably to the published values of a tunability of 6.7 pm/°C. The temperature used for the fit of the Spectra Physics diode is unknown. The different intercepts of 779.75 nm and 779.99 nm are likely associated with the diode chassis temperature related spectral shifts. A comparison to the experimental data and the Spectra Physics data is shown in Figure 12. A fit for the 20°C data is included for comparison but the Ocean Optics data suggests that this is not completely reliable. The fit obtained for the 37°C data was used for the remainder of the experiments to determine the wavelength output of the pump diode. This was especially important as the performance of the wavemeter deteriorated during the course of the experiments, failing altogether during the knife edge experiments.

Additionally, the slope efficiency of the diode was determined. The diode output power as a function of pump current at several temperatures is shown in Figure 13.

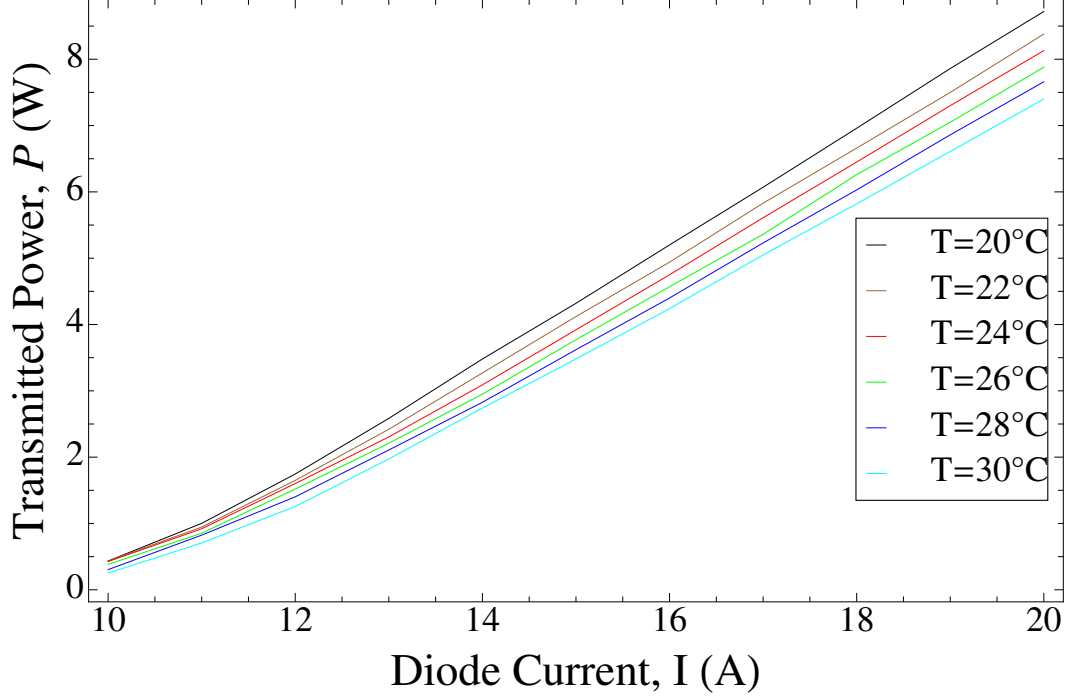


**Figure 13. Pump diode slope efficiencies for the 20°C to 30°C range. As the temperature increases, the slope efficiency decreases.**

Near the threshold current of approximately 10 A, the increase in power was exponential. Once the current reached 13 A, the growth of diode power as a function of current became linear through the range of currents tested. The temperature independence was investigated by increasing the current from 10 A to 20 A at temperatures of between 20°C and 30°C in 2°C increments. By analyzing the linear regime of each plot, it was determined that the slope efficiency increased from 0.773 W/A at 30°C to 0.878 W/A at 20°C, decreasing linearly with increasing temperature.

When the diode chassis temperature was raised to the operational temperature of 37°C, the slope efficiency dropped to 0.547 W/A, as shown in Figure 14.

### 4.3 Pump Beam Waist Characterization Analysis

To properly characterize a non-Gaussian beam with a knife-edge experiment, cross-sectional power profiles should be obtained for both  $x$ - and  $y$ -axes (*Interna-*

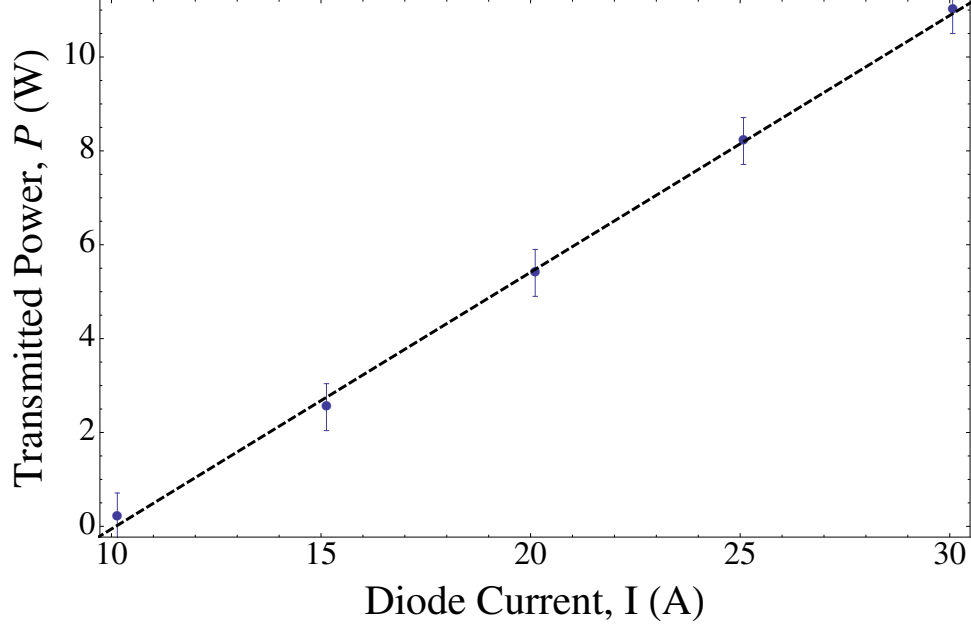


**Figure 14. Pump diode slope efficiency at 37°C. The slope efficiency of the pump diode at 37°C is 0.547 W/A.**

tional Organization for Standardization, 2005). Since there were no components to construct a dual-axis knife-edge apparatus with reliable mechanical repeatability to ensure the blade remained in a constant plane, a series of diagnostic cross sectional scans of the pump beam was performed at fiber stage mount rotation angles of 0°, 90°, 180°, and 270° to determine if rotating the fiber mount 90° would be effectively the same as performing a dual-axis knife-edge measurement. At each angle, knife-edge cross sections were obtained at  $z_R = 0$  mm, 15 mm, 30 mm, and 45 mm, using the focusing lens position as a reference for the  $z$ -axis. Since the position of the focusing lens can be varied along the  $z$ -axis and thereby change the location of the waist, the focusing lens was fixed. This illustrates the fact that the knife edge measurements and all subsequent analyses treat the high reflector as a constant. This is a reasonable assumption since any tilt adjustments will have a negligible effect on the  $z$ -axis position of the waist. Each measurement was started with the blade completely blocking the beam to keep heating of the pyrometer laser power meter head to a minimum.

This approach also had the additional benefit of minimizing the effects of systematic error from hysteresis caused by the translation stages used to position the blade.

### **Fiber Rotation Dependence.**

At first glance, the results of the diagnostic scans indicated separate  $x$  and  $y$  cross sections would be necessary. The  $0^\circ$  and  $90^\circ$  cross sections had incongruent crossover points near 35% of normalized power while the  $180^\circ$  and  $270^\circ$  shared incongruent crossover points near 25% of normalized power. Further investigation into this revealed an optical misalignment where neither the plane of the plano-convex lens was orthogonal to the beam propagation axis nor the beam propagation axis co-linear with the optical axis of the lens. This caused the center of the beam to move in an elliptical pattern as the fiber was rotated through  $360^\circ$ , shown in Figure 15. The power centroids were measured with the Coherent PowerMax power meter every  $10^\circ$ . Additionally, the repeatability of the effects of fiber rotation were tested by measuring the cross-sectional power profile of the pump beam with the fiber set to  $60^\circ$  in the rotation stage, rotated in a random fashion and then returned to  $60^\circ$  and measured again, denoted as red triangles in Figure 15. The power measurements were within the error bounds of one another.

### **Translational Corrections.**

The shifting beam centroid resulted in an angular error in the cross sectional power data. This error can be seen in Figure 16 as the beam centroid in the  $xz$ -plane moved in the positive  $x$  direction as  $z$  increased. Figure 16 also revealed an additional linear translational error in the data along the  $x$ -axis. As the blade's  $z$ -axis position was changed, the fitted beam center shifted back and forth along the  $x$ -axis, creating a zig-zag pattern. The pattern of the shift correlates to how the knife-edge apparatus

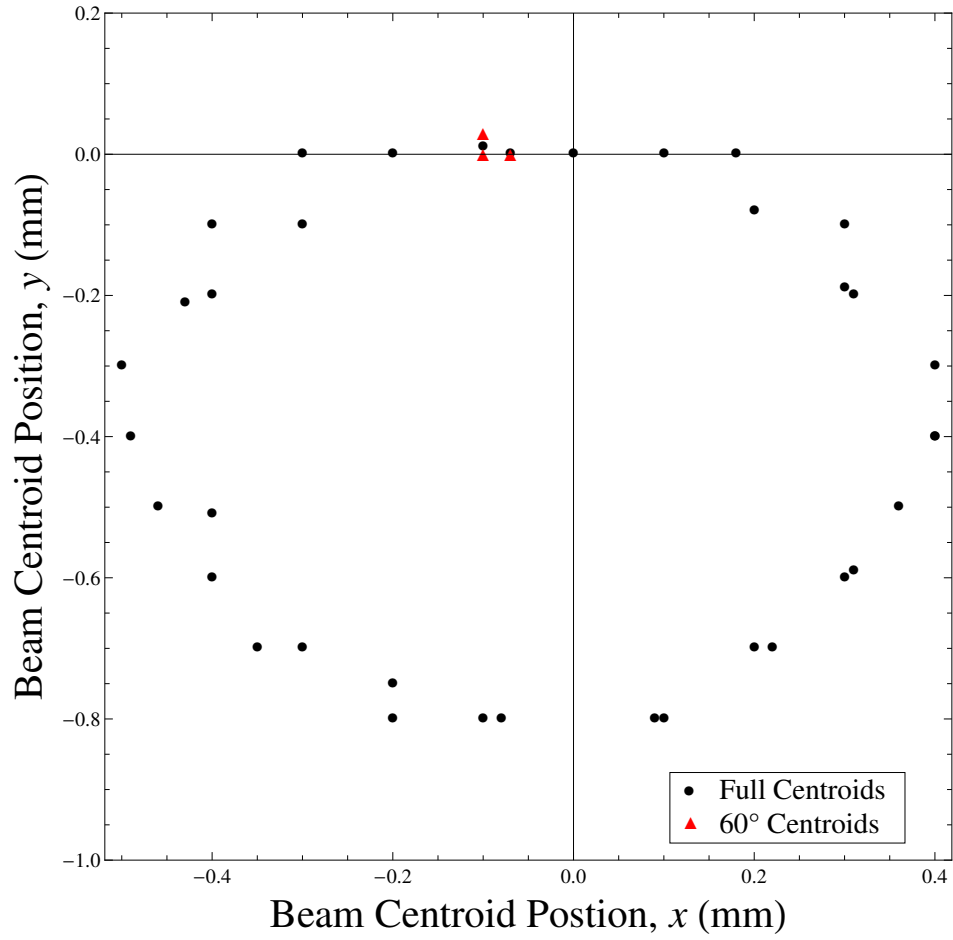


**Figure 15.** Effects of fiber rotation on beam centroid position. Rotating the pump diode fiber  $360^\circ$  changed the location of the pump beam centroid in an ellipse with an eccentricity of 0.46. Measurements taken at random of the centroid location at the  $60^\circ$  position, denoted by red triangles, showed good repeatability.

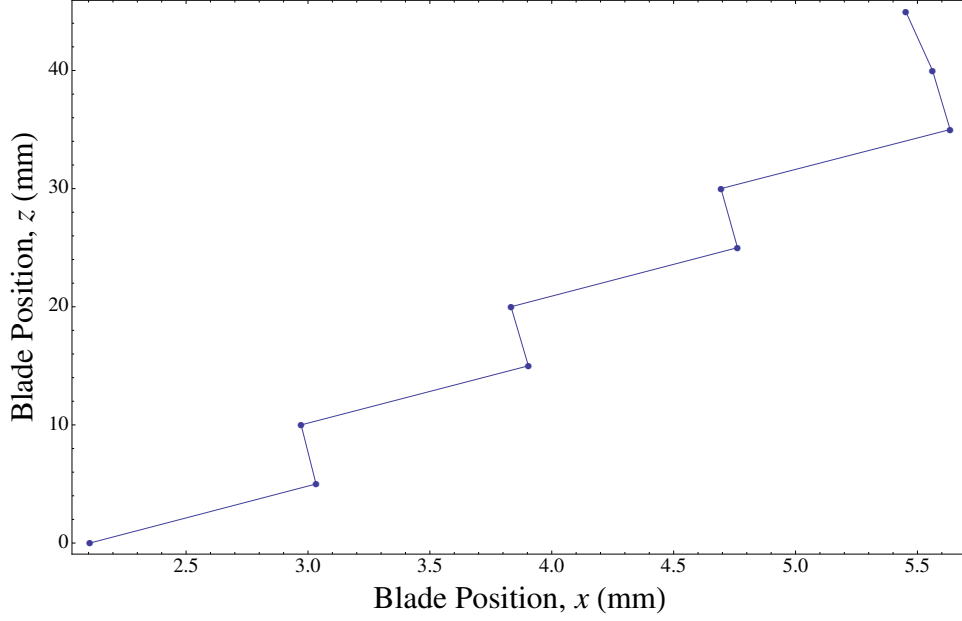


**Figure 16. Translational shifts in fitted beam centroids.**

was operated during the measurement: At  $z = 0$  mm, the blade was translated in the  $x$ -axis from 0 mm to 20 mm. The blade was then moved on the  $z$ -axis to  $z = 5$  mm and translated back on the  $x$ -axis from 0 mm to 20 mm and so on.

After an examination of the  $x$ -axis translation stage, the source of the  $x$ -axis error was determined to be the result of a hairline crack in the stage's leadscrew mount. The crack allowed the stage to shift slightly each time the leadscrew direction was reversed. This is supported by the fact that the sign of slope of the line in Figure 16 remains constant between the  $z = 40$  mm and  $z = 45$  mm measurements. The  $x$ -axis leadscrew was reset during the  $z = 45$  mm measurement, resulting in the same  $x$ -axis translation direction for both measurements.

Despite this, the error could be minimized. The overall slope of the line in Figure 16 indicated the propagation axis of the pump beam was not co-linear with the  $z$ -axis translation stage. Using the angle between the two axes and the eccentricity angle of the fiber rotation pattern and translational error to the data, a correction factor was applied to the  $x$ -axis power data. The results of the correction are plotted in Figure

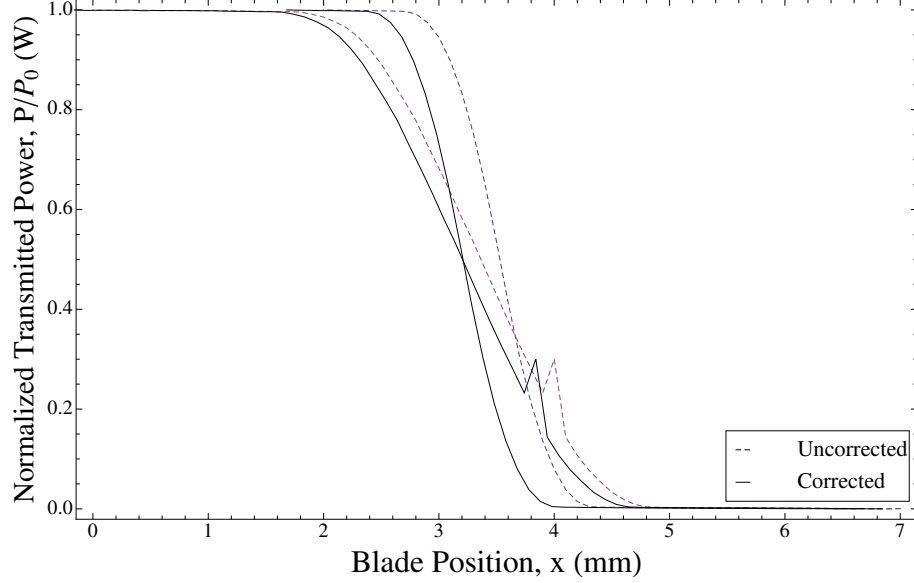


**Figure 17. Positional error correction in knife edge power profile data. Applying a correctional factor to the power profile data shifts the cross-over point between two separate power profiles (additional profiles were omitted for clarity) to the 50 percent mark, indicating the data is aligned along the beam propagation axis. The spikes in the data are the result of a combustion event on the surface of the blade.**

17 and shows the crossover points for the corrected and uncorrected scan data for two profiles spaced 5 mm apart. With the correction factor, the power crossover points for each scan coincided at 50% of the normalized transmitted power. The spikes in the data corresponded to burning events on the blade, resulting a brief surge in intensity.

The corrections in Figure 18 showed not only that the rotation of the fiber was a suitable analogue to a dual-axis knife edge measurement but that the beam structure was sufficiently uniform that a dual-axis measurement was not necessary.

The test scans also revealed a small rotational dependence on the pump beam power. This was expected since the beam is propagating from the diode bar to the cavity via a multimode fiber. Any stresses on the fiber result in birefringence effects and alter the path length of the beam as it propagates. This, in turn, changes the losses in the fiber. Ultimately, this particular dependence is irrelevant to the operation of this DPAL since the fiber rotation angle is set to the Brewster's angle with respect



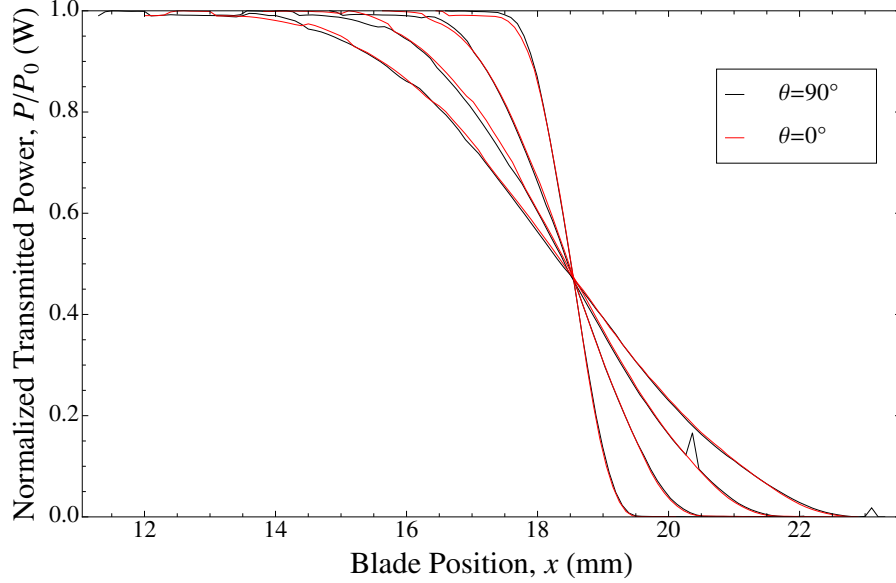


**Figure 18.** Comparison of knife edge power profile measurements for fiber rotation angles of  $0^\circ$  and  $90^\circ$ . The power profiles for  $0^\circ$  and  $90^\circ$  are almost identical, implying circular symmetry of the pump beam. The spikes in the data are the result of a combustion event on the surface of the blade.

to the gain cell to take advantage of the minor polarization of the pump beam. Once it was determined the beam possessed sufficient symmetry such that only an x-axis pass was necessary, a full, ten-pass knife edge measurement was conducted.

### Beam Waist Determination.

The first time the experiment was conducted, the range of  $z$  values fell short of the beam waist and though the experimental data produced what appeared to be good results for  $z_0$  and  $w_0$ , the experiment was conducted again after moving the knife edge translation apparatus to a location where the waist was expected to fall near the  $z = 20$  mm cross sectional pass. The fit is shown in Figure 19 and summarized in Table 2, where it should be noted that the  $z_0$  value is the waist location based on the location of the focusing lens.

The estimated location of  $w_0$  was determined by using burn paper to compare spot sizes at different  $z$  values. The fitted data reveals a waist location  $z_0 = 137$  mm,

**Table 2. Pump Beam Waist Characterization Results**

Parameter	Fit Estimate	Standard Error	Confidence Interval
$M^2$ (dimensionless)	131.5	6.5	116.2, 146.8
$w_0$ (mm)	0.036	0.001	0.033, 0.038
$z_0$ (mm)	136.6	0.2	136.2, 137.0

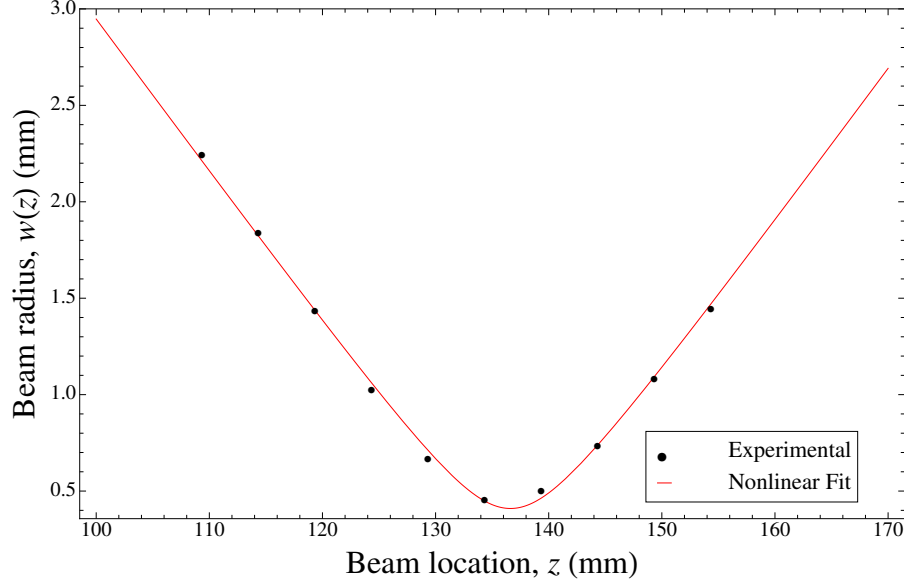


**Figure 19. Nonlinear fit to the pump beam power profile measurements. The beam location is shown with respect the focusing lens.**

very close to where it was predicted by earlier burn-paper tests. The quality factor  $M^2$  is 132, comparing well to the published value of 125. Taken with the  $M^2$  value, the real waist becomes 0.41 mm, compared to a published value of 0.35 mm from Petersen and Lane.

#### 4.4 Pump Beam Linewidth Characterization Experiment

At the beginning of the experiment, a background spectrum was recorded and subtracted from the subsequent spectra. As the VBG was scanned upwards from its lower bound, the upper wing of the pump beam altered the background of the spectral

features around the  $D_1$  emission line. This changed the background of each spectrum and the degree of change increased as the VBG output wavelength increased. Since the region of interest on each spectrum was a 10 nm window from 790 nm to 800 nm, the change in background appeared as a linear shift. By creating a linear fit of the upper wing of the pump diode emission line for each spectrum, the increase in background caused by the pump diode output was removed. Each spectrum was then analyzed to determine the integrated intensity of the  $D_1$  emission by generating a nonlinear fit to each spectrum and integrating over the 10 nm window. Due to the presence of the nearby pump spectral line, the small sampling window for the  $D_1$  line, and limited resolution of the spectrometer, fitting the spectra was extremely problematic. In the end, a Gaussian fit was used to determine the integrated intensity. It should be noted that simply summing the peaks produced an integrated intensity close to that of the value obtained using the Gaussian fit.

The integrated intensities were then plotted according to wavelength and fitted to a Lorentzian lineshape using the Experimental Data Analysis package in *Mathematica*. A Lorentzian lineshape was used since it was assumed that pressure broadening would be the dominant line-shaping process. For the 100°C data, fitting the linewidth data produced a predicted line center of 780.25 nm, as opposed to a  $D_1$  wavelength 780.24 nm (*Steck*, 2001), and a linewidth of 0.12 nm. The fitted lineshape equation is

$$g(\nu) = \frac{2.62}{0.0045 + (\lambda - 780.22)^2} \quad (20)$$

and the fitted data is shown in Figure 20. The asymmetrical structure of the original fluorescence spectra results in a relatively poor fit as evidenced by the fit residuals in the inset. The structure in the lower ends of the residuals may be indicative of the shoulder on the pump beam spectra that can be seen in Figure 11. The results from the other temperature sets are shown in Table 3. With a wavemeter resolution

of 0.01 nm, the average linewidth is 0.12 nm and the average center wavelength is 780.23 nm.

**Table 3. Pump Beam Linewidth Measurement Results**

<b>Cell Temperature (°C)</b>	<b>FWHM (nm)</b>	<b>FWHM Fit Error</b>	<b>Wavelength (nm)</b>	<b>Wavelength Fit Error</b>
100	0.11525	0.00017	780.254	0.000057
105	0.11994	0.00015	780.220	0.000051
110	0.12983	0.00011	780.222	0.000037
115	0.13359	0.00008	780.223	0.000028

Assuming a pressure broadening coefficient of 20 MHz/Torr, the 500 Torr test cell would be expected to have an absorption linewidth of approximately 10 GHz. The observed lineshape has a width of 59 GHz and is dominated by the diode lineshape. The obtained linewidth value represents the width of the convolution of the pump beam linewidth and absorption linewidth of the rubidium gain medium, rather than the linewidth of the diode itself. Without further experiments, this obtained value of 0.12 nm can only be considered as the lower bound for the linewidth of the pump diode.

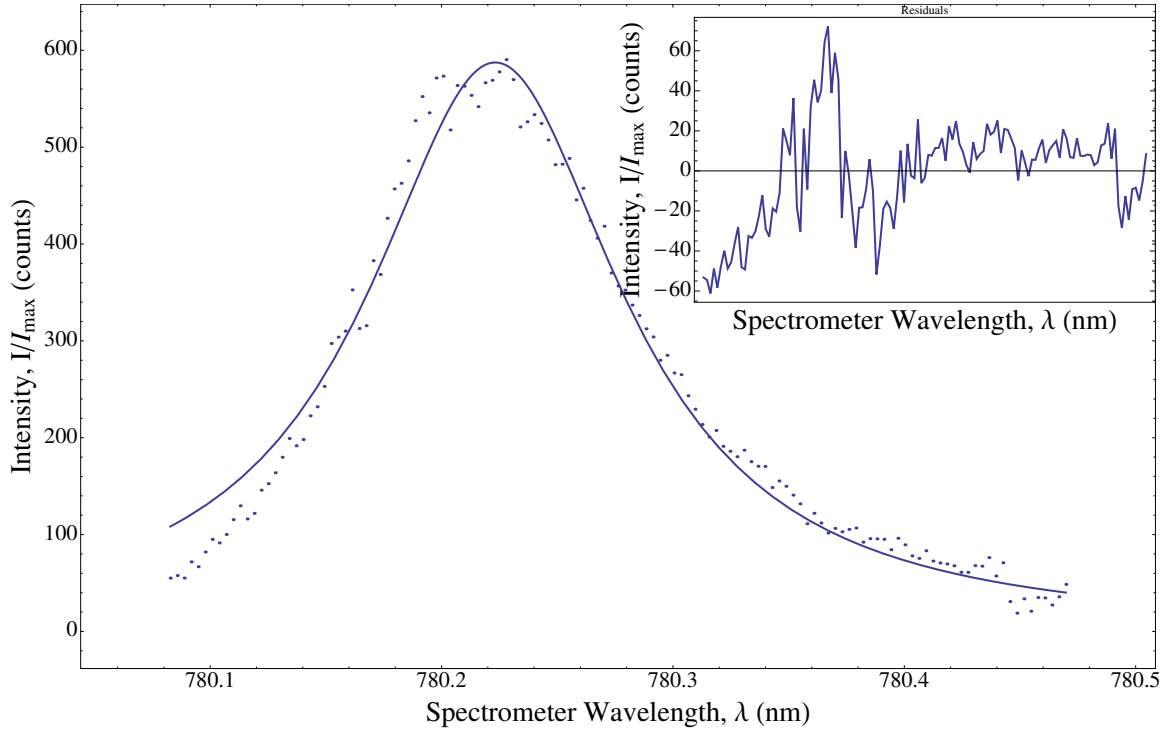


Figure 20. Nonlinear fit to the pump beam linewidth. The asymmetry of the fit is due to the non-uniform distribution of emission wavelengths at the 780 nm pump line. The inset is a plot of the residuals of the fitting routine.

## V. Conclusions and Recommendations

### 5.1 Chapter Overview

This chapter consists of two sections. The first section summarizes the results of the characterization experiments. The second section discusses the next steps for the Spectra Physics DPAL.

### 5.2 Conclusions

The experimental data favorably matches the Spectra Physics values and increases the confidence that the assumptions listed in Section 1.4 are correct. Although access to a higher resolution spectrometer would refine these numbers, it is not necessary with the exception of the diode linewidth. From a resonator context, the critical parameters are now established for the pump source. The results are summarized in Table 4.

Also, significant work was performed to determine how to operate the laser diode and the VBG. This will be crucial for future research and the operating parameters can be found in Appendix 1.

**Table 4. Spectra Physics DPAL Pump Diode Operating Parameters**

Characteristic	Operating Value	Spectra Physics Value
Pump Beam Waist, $w_0$ (mm)	0.41	0.35
Pump Beam $M^2$	132	125
VBG Tuning Rate (pm/°C)	6.1	6.7
Diode Operating Temperature (°C)	37	N/A
Diode FWHM (nm)	0.12 (Lower Bound)	0.1
Diode Slope Efficiency (W/A)	0.547	N/A

### 5.3 Recommendations for Future Work

The next step in this effort is to bring the DPAL to an initial operating capacity in the  $\text{TEM}_{00}$  mode in order to establish a baseline for resonator performance. The second step is to explore new gain cells to take advantage of the diode's high power output and minimize the chance of destroying the gain cells due to minor misalignments.

The pump diode exhibits a beam waist of 0.41 mm and exceeds the maximum  $\text{TEM}_{00}$  beam width of the DPAL's semi-hemispherical cavity of  $w(30\text{ cm}) = 0.39$  mm. This means the DPAL resonator, as designed, cannot oscillate purely in the  $\text{TEM}_{00}$  mode. To achieve  $\text{TEM}_{00}$  output, the waist of the pump beam must be matched to the  $\text{TEM}_{00}$  mode volume of the resonator. This can be accomplished by changing the radius of curvature of the output coupler and also by changing the cavity length to increase the waist of the resonator so the diameter of the resonator's  $\text{TEM}_{00}$  beam matches the waist of the pump diode. Similarly, the waist of the pump beam can be reduced by decreasing the focal length of the focusing lens (component D in Figure 1).

The small physical dimensions of the gain cell presents several problems. First, the location of the cell within the resonator is critical to ensure the beam waist is located inside the gain medium. Second, the cell must be heated to generate a sufficient rubidium population for lasing to occur. Given the potential for pump intensities that can exceed  $10\text{ kW/cm}^2$ , there is a probability of inducing unwanted photochemistry in the gain medium such as the formation of rubidium hydrides, hydrocarbon soot, and damage to the optical surfaces of the cell. A new, longer cell would permit the generation of the necessary rubidium population at a lower temperature, thereby minimizing the risk of a catastrophic event.

## Appendix A. Spectra Physics J80 Diode Controller Operations

### 1.1 Communications Settings

The Spectra Physics DPAL pump diode has two separate command interfaces: one for the diode and one for the VBG. The J80 diode controller contains a standard diode temperature and power controller that is used to command and monitor the diode current and chassis temperature. The second controller is used to command and monitor the VBG. Both controllers are located in the J80 assembly. Each controller is accessible over the J80 USB port using a scripting language or by direct command using a serial interface program such as Hyperterminal. During the experiments, the diode and VBG were controlled via Hyperterminal using the following settings listed in Table 5.

**Table 5. Communications Settings for the J80 Controller**

Setting	Diode	VBG
COM Port	3	4
Bits per second	9600	19200
Data bits	8	8
Parity	N	N
Stop bits	1	1
Flow control	None	None

### 1.2 Commands and Syntax

The J80 diode controller is the primary interface to the laser diode. It allows the user to control the current of the laser diode and temperature of the laser diode chassis. Both parameters can be changed and monitored by sending commands directly through the serial link. Additionally, the J80 features a small display screen that reports the immediate values of the current and temperature.



When changing the diode current, the J80 does not gradually change the current. For instance, if the current is changing from 0 A to 20 A, it will jump immediately from 0 A to 20 A. This can potentially harm the diode so the user is advised to incrementally raise and lower the current by sending current-changing commands in 1 A increments. This process can be automated by using a scripting utility.

Changes to the diode temperature do not require incremental commands. The J80 will gradually increase or decrease the temperature. When changing the temperature of the diode, the diode should be given several minutes to stabilize before frequency-critical experiments are being conducted.

A full description of the command syntax and available commands are listed on the following pages. The list was obtained using the HELP command.

**J80 COMMAND LIST**

Syntax: ['?']&lt;command&gt;[&lt;n&gt;][':']&lt;argument&gt;]&lt;r&gt;

Syntax	Interpretation
[]	encloses an optional item
?	is used to query a diode or box
<command>	is any system command
<n>	is an integer representing a diode
:	is the delimiter between diode or box and its data
<arg>	is the data of any type for the diode or box
<r>	is carriage return or enter

Syntax Example	Interpretation
stack:1<r>	place all boxes in stack mode
on<r>	turn on all diodes in stack
c1:41.5<r>	adjust diode_1 of box_1
c2:42.5<r>	adjust diode_2 of box_1
c3:43.5<r>	adjust diode_1 of box_2
c4:44.5<r>	adjust diode_2 of b
?pu<r>	query UV power
?config<r>	query config for box1
?config2<r>	query config for box2
spl1:1=splash line_1 text<r>	set splash text for box_1/line_1

COMMAND	ACCESS	DESCRIPTION
ACC	get/set	auto calibrate coarsen
ALIGN	get	toggle harmonic crystal Align mode
AT	get/set	AutoTemp toggle
ATR	get/set	AutoTemp rate
BAUDRATE	get/set	RS232 baudrate
BCT	get/set	Backwards compatibility emulator mode
BR	get/set	RS232 baudrate
C	get/set	diode current
CABTEMP	get	cabinet temperature
CAL	get/set	calibrate uv reading
CALC	get	diode calibration current
CALHRS	get	diode calibration hours
CALT	get	diode calibration temperature
CE	get	harmonic crystal edges
CONFIG	get	system configuration
CONFIGSUPSET	set	initiate Ymodem-based partial config upload
CONT	get/set	auto calibrate
CPUMODULE	get	which CPU is installed?

COMMAND	ACCESS	DESCRIPTION
CR	get/set	command responding toggle
CS	get	diode current setpoint
D	get/set	system on or off
DCL	get	diode current limit
DITH	get	dither on/off
DITHSAMP	get	dither samples
DITHGAIN	get	dither gain
DITHSTEP	get	dither step
DITHRATE	get	dither rate
DH	get	diode hours
DOT	get	diode calibration temperature
DP	get	diode photocell
DSN	get	diode serial number
DSD	get	diode shipdate
ECHO	get/set	set the
F	get	active faults
FH	get	fault/state history
FHG	get	FHG crystal temperature
FHGD	get/set	FHG crystal temperature DAC
FHGE	get	FHG crystal temperature error
FHGSPOTSIZE	get	FHG spot size
FREQ	get	PC104 Frequency for QSwitch
G	get/set	Q-switch gate open toggle
H	get	fault/state history
HCS	get	has crystal-shifter toggle
HEADHRS	get	IR head hours
HEADHRSUV	get	UV head hours
HEADSN	get	head serial number
HELP	get	this listing of commands and their descriptions
HINDI	get/set	toggle indicators on/off
HMODEL	get	harmonic model
HO	get/set	harmonic options
HQ	get	has Q-switch toggle
HRFDET	get	has RF detector toggle
HS	get	diode heat-sink temperature
HSWWT	get/set	Heat sink high temp warning temperature
HSLL	get	diode heatsink lower limit
HSUL	get	diode heatsink upper limit
HTT	get	
LES	get	load ee shutter at next boot
LEH	get	load ee harmonic at next boot
LG	get	power-servo lock gain
LW	get	power-servo lock window
M	get/set	laser mode
MSAVEON	get/set	manual parameter save

COMMAND	ACCESS	DESCRIPTION
MSAVE	set	do manual parameter save
MODUSN	get	harmonic module serial number
MODEL	get	model number
ND	get	number of diodes
ON	get/set	system on
OFF	get/set	system off
P	get/set	IR power
PG	get/set	green power
PGM	get	max green power
PIM	get	IR max power scale
PIRM	get	max IR lightloop power
PB	get	passbank current rating
PL	get	diode pump limit
POW	get	
PRF	get/set	Q-switch repetition rate
PRFMIN	get	Q-switch repetition rate min
PROMPT	get/set	prompt-control toggle
PS	get	laser power setpoint
PSSN	get	power supply serial number
PU	get/set	UV power
PUM	get	max UV power
PWRSERVO	get	laser power servo state
PWS	get	laser power setpoint
Q	get/set	Q-switch repetition rate
QMIN	get	Q-switch repetition rate min
RFDETCNF	get/set	RF detector config
S	get	system status/fault
SC	get/set	Q-switch FPS current
SERHRS	get	service hours
SG	get	power-
SHG	get	SHG crystal temperature
SHGD	get/set	SHG crystal temperature DAC
SHGE	get	SHG crystal temperature error
SHT	get/set	laser shutter open
SL	get	power-servo step limit
SPL	get/set	splash line
SPLASH	get/set	splash-at-boot toggle
SPOT	get/set	spot on harmonic crystal
SPOTHRS	get	spot usage hours
SPOTPAT	get	spot pattern for harmonic crystal
SSD	get	system shipdate
ST	get/set	Q-switch FPS time
STACK	get/set	Stack setup
STB	get/set	Q-switch FPS current
SUP	get/set	Q-switch FPS time

COMMAND	ACCESS	DESCRIPTION
T	get/set	
TT	get	tower temperature
TCMD	get/set	t-series compatibility toggle
THG	get	THG crystal temperature
THGD	get/set	THG crystal temperature DAC
THGE	get	THG crystal temperature error
TS	get	diode temperature setpoint
UPGRADE	set	initiate Ymodem-based software upgrade
V	get	software version
VFH	get	verbose fault/state history
VV	get	verbose software version
X	get	legacy (t-series) diode storage

## Appendix B. Volume Bragg Grating Operations

### 2.1 Overview

The VBG temperature controller is based on a Burr-Brown DAC7641U digital-to-analog converter (DAC). It features a 16-bit digital input, with a range from 0000 to 4000, and generates an output voltage proportional to the digital input. The output is used to control the current to the thermoelectric element on the VBG assembly (Figure 6). Feedback is provided by a temperature sensor mounted on the VBG assembly.

To change the temperature of the VBG, a digital input is sent to the VBG temperature controller over a serial input link. A value of 0001 corresponds to a temperature step of  $0.02^{\circ}\text{C}$ , giving the controller a range of  $0^{\circ}\text{C}$  to  $80^{\circ}\text{C}$ . The VBG should not be taken below  $15^{\circ}\text{C}$  to minimize the risk of condensation. For the Spectra Physics DPAL, the relationship between the VBG output wavelength and the DAC digital input is given by

$$\lambda_{\text{exp}(37^{\circ}\text{C})} = 779.99\text{nm} + (1.21 \times 10^{-4}\text{nm}/\text{step}) \times \text{DAC} \quad (21)$$

where  $\text{DAC}$  is the digital input (0000-4000).

The temperature controller contains four DAC channels and twelve analog-to-digital (ADC) channels that can be monitored. The state of each channel can be polled directly over the serial link. For the operation of the laser, the relevant channels are DAC:2 and ADC:8. The temperature of the VBG is changed by sending a digital input command to DAC:2. The actual temperature of the VBG is monitored by polling the status of ADC:8. The output of ADC:8 is in the form of a digital input. To obtain the temperature, it must be multiplied by  $0.02^{\circ}\text{C}$ . A full description of the command syntax and available commands are contained at the end of this appendix.

## 2.2 Syntax Issues

When using Hyperterminal to command the VBG, a condition may occur where the user can inadvertently change the settings of the DAC on the VBG temperature controller. When entering a command in Hyperterminal to change the value of DAC:2, the command is "DAC:2:XXXX", where "XXXX" is the digital input corresponding to the desired VBG temperature. If the next command is in the format "DAC:Y", where "Y" is the address of the DAC, Hyperterminal will send "DAC:Y:XXXX". An example of this is shown in Figure 21. In this example, the user attempts to change the DAC:2 state to a digital input value of 1500 and then poll the status of DAC:0. Figure 21 (A) shows the correct input stream. If the "?" is absent from the "?DAC:0" command as shown in (B), DAC:0 will inherit the same digital input value as DAC:2 (C). This software error can be avoided by pressing the ENTER key twice after entering each command.

Command	Comment
(A)	
> DAC:2:1500	Set DAC:2 state to 1500
> ?DAC:0	Query the state of DAC:0
> 2048 DAC:0	DAC:0 set to 2048
(B)	
> DAC:2:1500	Set DAC:2 state to 1500
> DAC:0	Erroneous input
(C)	
> ?DAC:2	Query the state of DAC:2
> 1500 DAC:2	DAC:2 set to 1500
> ?DAC:0	Query the state of DAC:0
> 1500 DAC:0	DAC:0 set to 1500

Figure 21. VBG Hyperterminal Command Anomaly Example. The user input is denoted in BLUE and system output is RED. Hyperterminal automatically indents the command line. In (A), the user enters a command to change the DAC:2 state. In (B), the user enters the same DAC:2 command as in part (A) but incorrectly enters the command to query DAC:0. Part (C) shows the result of the software error.



## VBG COMMAND LIST

Syntax Example	Interpretation
?ADC:3	query status of ADC at address 3
DAC:2:3500	set input level of DAC at address 2 to 3500

COMMAND	ACCESS	DESCRIPTION
?ADC:XX	get	Poll status of ADC at address XX
?DAC:XX	get	Poll status of DAC at address XX
DAC:XX:YYYY	set	Set input level YYYY of DAC at address XX

Operational Notes
<p>The temperature of the VBG is set using DAC:2. The range of values for DAC:2 is 0-4000 steps with a resolution of 0.02°C/step, giving a temperature range of 0°C to 80°C. If the user wanted to set the temperature of the VBG to 30°C, the command would be "DAC:2:1500". The actual output level of the temperature controller can be monitored via ADC:8 using the command "?ADC:8". This value should be within a few steps of the DAC:2 state.</p>

## Bibliography

- Bogachev, A. V., S. G. Garanin, A. M. Dudov, V. A. Yeroshenko, S. M. Kulikov, G. T. Mikaelian, V. A. Panarin, V. O. Pautov, A. V. Rus, and S. A. Sukharev, Diode-pumped caesium vapour laser with closed-cycle laser-active medium circulation, *Quantum Electronics*, 42, 95–98, 2012.
- Brown, K. C., and G. P. Perram, Spin-orbit relaxation and quenching of cesium  $5^2p$  in mixtures of helium, methane, and ethane, *Phys. Rev. A.*, 85, 2012.
- Ciapurin, I. V., L. B. Glebov, and V. I. Smirnov, Modeling of Gaussian beam diffraction on volume Bragg gratings in PTR glass, *Proc. of SPIE*, 5742, 183–194, 2005.
- Glebov, A. L., O. Mokhun, A. Rapaport, S. Vergnole, V. Smirnov, and L. B. Glebov, Volume Bragg gratings as ultra-narrow and multiband optical filters, *Proc. of SPIE*, 8428, 2012.
- Hager, G. D., and G. P. Perram, A three-level analytic model for alkali metal vapor lasers: Part I. Narrowband optical pumping, *App. Phys. B.*, 101, 45–56, 2010.
- International Organization for Standardization, Lasers and laser-related equipment - Test methods for laser beam widths, divergence angles and beam propagation ratios - Part 1: Stigmatic and simple astigmatic beams, ISO 11146-1, 2005.
- Krupke, W. F., R. J. Beach, V. K. Kanz, and S. A. Payne, Resonance transition 795-nm rubidium laser, *Optics Letters*, 28, 2336–2338, 2003.
- Petersen, A., and R. Lane, Second harmonic operation of diode-pumped Rb vapor lasers, *Proc. of SPIE*, 7005, 2008.
- Siegman, A. E., *Lasers*, University Science Books, Sausalito, CA, 1986.
- Siegman, A. E., Defining, measuring and optimizing laser beam quality, *Proc. of SPIE*, 1868, 1993.
- Steck, D., Rubidium 87 D Line Data, *Tech. rep.*, Los Alamos National Laboratory, 2001.
- Verdeyen, J. T., *Laser Electronics*, Prentice Hall, Upper Saddle River, NJ, 1995.
- Zameroski, N. D., G. D. Hager, W. Rudolph, and D. A. Hostutler, Experimental and numerical modeling studies of a pulsed rubidium optically pumped alkali metal vapor laser, *J. Opt. Soc. Am. B*, 28, 1088–1099, 2011.

## Vita

Master Sergeant Chad Taguba was born at Sheppard AFB, Texas. After graduating from Berkmar High School in 1991, he began studying physics at the Georgia Institute of Technology prior to enlisting in the Air Force in 1994. He resumed his academic pursuit in physics in 2003 and graduated with a Bachelor of Science Degree in Physics in May 2007 from Angelo State University.

Master Sergeant Taguba has completed nearly nineteen years of active duty service, most of which has been with the Air Force Technical Applications Center (AFTAC). He enlisted as a 9S000 Systems Repair Technician and reported to his first duty station, the Technical Operations Division, McClellan AFB, CA, in February 1995 as an Atmospheric Research Equipment Technician. In August 1998, he became an Electro-Optics Technician for the Advanced Technology Directorate, AFTAC, Patrick AFB, FL. He left AFTAC in 2003 to teach physics as a technical training instructor for the Reporting Identifier 9S100 at Goodfellow AFB, TX. He returned to AFTAC in 2007 as the Superintendent of the Nuclear Sciences Division, Materials Technology Directorate. In 2011, he entered the Graduate Applied Physics program, School of Engineering, Air Force Institute of Technology to obtain a Master's Degree in physics. Upon graduation, Master Sergeant Taguba will return to AFTAC as the Superintendent, Radiochemistry Laboratory.

# REPORT DOCUMENTATION PAGE

Form Approved  
OMB No. 0704-0188

The public reporting burden for this collection of information is estimated to average 1 hour per response, including the time for reviewing instructions, searching existing data sources, gathering and maintaining the data needed, and completing and reviewing the collection of information. Send comments regarding this burden estimate or any other aspect of this collection of information, including suggestions for reducing this burden to Department of Defense, Washington Headquarters Services, Directorate for Information Operations and Reports (0704-0188), 1215 Jefferson Davis Highway, Suite 1204, Arlington, VA 22202-4302. Respondents should be aware that notwithstanding any other provision of law, no person shall be subject to any penalty for failing to comply with a collection of information if it does not display a currently valid OMB control number. **PLEASE DO NOT RETURN YOUR FORM TO THE ABOVE ADDRESS.**

<b>1. REPORT DATE</b> (DD-MM-YYYY) 04-03-2013		<b>2. REPORT TYPE</b> Master's Thesis		<b>3. DATES COVERED</b> (From — To) Aug 2011 — Mar 2013	
<b>4. TITLE AND SUBTITLE</b>  Pump Diode Characterization for an Unstable Diode-Pumped Alkali Laser Resonator				<b>5a. CONTRACT NUMBER</b>	
				<b>5b. GRANT NUMBER</b>	
				<b>5c. PROGRAM ELEMENT NUMBER</b>	
<b>6. AUTHOR(S)</b>  Taguba, Chad T., MSgt				<b>5d. PROJECT NUMBER</b>	
				<b>5e. TASK NUMBER</b>	
				<b>5f. WORK UNIT NUMBER</b>	
<b>7. PERFORMING ORGANIZATION NAME(S) AND ADDRESS(ES)</b> Air Force Institute of Technology Graduate School of Engineering and Management (AFIT/EN) 2950 Hobson Way WPAFB OH 45433-7765				<b>8. PERFORMING ORGANIZATION REPORT NUMBER</b>  AFIT-ENP-13-M-33	
<b>9. SPONSORING / MONITORING AGENCY NAME(S) AND ADDRESS(ES)</b> HEL Joint Technology Office 801 University Blvd. SE, Suite 209 Albuquerque, NM 87106 Phone: 505-248-8208 Email: harro.ackermann@jto.hpc.mil				<b>10. SPONSOR/MONITOR'S ACRONYM(S)</b>  HELJTO	
				<b>11. SPONSOR/MONITOR'S REPORT NUMBER(S)</b>	
<b>12. DISTRIBUTION / AVAILABILITY STATEMENT</b>  APPROVED FOR PUBLIC RELEASE; DISTRIBUTION UNLIMITED.					
<b>13. SUPPLEMENTARY NOTES</b>					
<b>14. ABSTRACT</b> Measurements of wavelength tunability, spectral linewidth, minimum spot size, and $M^2$ were made for a rubidium diode-pumped alkali laser (DPAL) containing a volume Bragg grating (VBG) for resonator characterization. The output wavelength of the pump diode was measured as a function of volume Bragg grating temperature. A linear relationship was observed that corresponded to an output wavelength range of $780.08 \text{ nm} \pm 0.01 \text{ nm}$ to $780.49 \text{ nm} \pm 0.01 \text{ nm}$ with a tuning rate of $6.1 \text{ pm}/^\circ\text{C}$ for a diode chassis temperature of $37^\circ\text{C}$ . Rubidium $D_1$ fluorescence spectra were recorded as the diode wavelength was scanned across its full range in 3 pm steps. The integrated intensities of the $D_1$ fluorescence peaks were used to generate a fit to a Lorentzian lineshape with line center at 780.23 nm and a FWHM of 0.12 nm. A knife-edge experiment measured the power profiles of the pump diode beam along a 4.5 cm beam path. The pump diode $M^2$ was determined by a nonlinear model fit to be 132, resulting in a minimum spot size of 0.41 mm. These results enable the pump diode to be matched with a alkali gain media for the validation of unstable DPAL resonator designs.					
<b>15. SUBJECT TERMS</b>  Diode Pumped Alkali Laser, Volume Bragg Grating, Unstable Resonator					
<b>16. SECURITY CLASSIFICATION OF:</b>			<b>17. LIMITATION OF ABSTRACT</b>	<b>18. NUMBER OF PAGES</b>	<b>19a. NAME OF RESPONSIBLE PERSON</b>
<b>a. REPORT</b>	<b>b. ABSTRACT</b>	<b>c. THIS PAGE</b>			Dr. Glen P. Perram, AFIT/ENP
U	U	U	U	62	<b>19b. TELEPHONE NUMBER</b> (include area code) (937) 255-3636, x4504; glen.perram@afit.edu